Performance assessment of the Water Enhanced Turbofan engine

Aerospace Science and Technology 178 (2026) 112389

Contents lists available at ScienceDirect

Aerospace Science and Technology

journal homepage: www.elsevier.com/locate/aescte

Original article

Performance assessment of the Water Enhanced Turbofan engine

Filip Herbertsson [a,*], Xin Zhao [a], Anders Lundbladh [a,b], Tomas Grönstedt [a]

[a] Department of Mechanical Engineering, Chalmers University of Technology, Hörsalsvägen 7A, 41258, Göteborg, Sweden
[b] GKN Aerospace Sweden, Flygmotorvägen 1, 46181, Trollhättan, Sweden

ARTICLE INFO

Communicated by Cummings Russell

Keywords:
Water Enhanced Turbofan
Cheng cycle
Heat recovery systems
Steam injection
Sustainable aviation
Fuel burn

ABSTRACT

An engine performance model of the Water Enhanced Turbofan (WET) is developed. The parametric analysis includes water-air ratio (WAR), turbine inlet temperature (TIT), overall pressure ratio (OPR), bypass ratio (BPR), fan pressure ratio (FPR) and six additional heat exchanger design parameters. An A350/XWB-type reference aircraft is modeled to quantify installation effects via cruise specific range. A 9.6% reduction in cruise TSFC is achieved, with a maximum reduction potential of 12.9% based on a Chilton-Colburn performance bound. However, once additional heat exchanger pressure losses, weight, and increased engine size are accounted for, no improvement in cruise specific range could be observed. Notably, the engine weight is expected to increase with 66% and the nacelle length and diameter are expected to increase with 22% and 40%, respectively, for which the condenser dominates the added heat exchanger volume. The study further highlights challenges that emerge from inherent features of the WET cycle. While higher WAR improves cruise specific range, it becomes increasingly difficult to limit TIT during take-off because reduced water recovery at elevated ambient temperature requires compensating by increasing TIT. The option of carrying additional water is evaluated as an alternative remedy, showing that for high-WAR designs more than $20\,\mathrm{kg\,s^{-1}}$ of water may be required at take-off. A further challenge with the WET cycle is that as WAR increases, core specific power rises, slowing the temperature drop across the turbines. Consequently, the cooling requirement extends further into the turbine system and may require cooling of multiple low-pressure turbine stages in the WET cycle.

1. Introduction

Aviation is currently responsible for 4.9% of anthropogenic radiative forcing [1], and the sector is growing each year. In 2019, before the COVID-19 pandemic, the number of p assengers increased by 3.6% [2] and the number of passenger-kilometers increased by 4.9% [2], further increasing emissions from the sector. Historical trends show an improvement in fuel efficiency of 24% [3] between 2005 and 2017, giving an annual improvement in fuel efficiency of 1.8%. Looking ahead from 2016, the International Civil Aviation Organization (ICAO) expects an annual decrease in fuel burn by 1.4% to 2050 [4]. Thus, market growth is expected to continue to outpace fuel efficiency improvements, leading to a net increase in carbon dioxide (CO_2) emissions. Furthermore, non-CO_2 emissions, such as nitrogen oxides (NO_X) and contrails, also contribute to global warming. Gradual improvement of existing technology is therefore not sufficient to achieve a net reduction in emissions from the sector. New innovative systems and sustainable fuels are required, if the goals of the Paris Agreement are to be met [5].

One promising innovation for reducing climate impact from aviation is the Water Enhanced Turbofan (WET) cycle. This propulsion concept enhances fuel efficiency by recovering waste heat after the turbines, while also increasing the specific heat capacity of the core stream. It was first proposed by Schmitz et al. in a series of studies on future engine cycles [6–8]. The WET cycle is a combination of an open Joule-Brayton turbofan cycle, running on air, and a quasi-closed Clausius-Rankine cycle, running on water. This type of combined cycle is also referred to as the Cheng cycle [9]. The WET cycle is illustrated in Fig. 1. Steam is injected into the combustion chamber, and is condensed after the last turbine stage by means of two heat exchangers. The first heat exchanger is placed after the last turbine stage, and is called the vaporizer. It transfers heat between the core flow and the liquid water stream, vaporizing the water and returning heat back into the combustion chamber. The second heat exchanger further cools the core flow by transferring heat

* Corresponding author.
E-mail addresses: filip.herbertsson@chalmers.se (F. Herbertsson), xin.zhao@chalmers.se (X. Zhao), anders.lundbladh@gknaerospace.com (A. Lundbladh), tomas.gronstedt@chalmers.se (T. Grönstedt).

https://doi.org/10.1016/j.ast.2026.112389
Received 6 October 2025; Received in revised form 26 January 2026; Accepted 16 April 2026
Available online 19 April 2026

Nomenclature

Abbreviations

A350	Airbus A350-900
BPR	Bypass ratio
FAR	Fuel-air ratio
FPR	Fan pressure ratio
HPC	High pressure compressor
HPT	High pressure turbine
ICAO	International Civil Aviation Organization
IPC	Intermediate pressure compressor
IPT	Intermediate pressure turbine
ISA	International standard atmosphere
LMTD	Logarithmic mean temperature difference
LPT	Low pressure turbine
LTO	Landing and take-off
MTOW	Maximum take-off weight
OPR	Overall pressure ratio
TIT	Turbine inlet temperature
TSFC	Thrust-specific fuel consumption
WAR	Water-air ratio
WET	Water enhanced turbofan
WRF	Water recovery factor

Roman symbols

A	Frontal area; [m^2]
A_r	Aspect ratio; [-]
C_{D0}	Parasite drag coefficient; [-]
c_p	Specific heat capacity; [$J\,kg^{-1}\,K^{-1}$]
c_T	Thrust-specific fuel consumption; [$mg\,N^{-1}\,s^{-1}$]
d	Nacelle diameter; [m]
F	Step size optimization parameter; [-]
f	Friction factor; [-]
j	Colburn factor; [-]
$K_{L/D}$	Lift-drag constant; [-]
l	Nacelle length; [m]
ℓ	Undisturbed flow length; [m]
L/D	Lift-drag ratio; [-]
$l_f/\sqrt{t_f}$	Fin characteristic length; [m]
$\dot{m}$	Mass flow rate; [$kg\,s^{-1}$]
M	Mach number; [-]
p_0	Stagnation pressure; [bar]
Δp	Pressure drop across flow channel; [%]
$\dot{Q}$	Heat transfer; [MW]
r	Random number; [-]
r_{lim}	Random number optimization parameter; [-]
R_s	Specific range; [$m\,kg^{-1}$]
S	Aircraft area; [m^2]
t_W	Wall thickness; [mm]
T_0	Stagnation temperature; [K]
ΔT_{pinch}	Pinch-point temperature difference; [K]
w	Weight; [N]
$\dot{W}$	Power; [MW]
$\mathbf{x}$	Optimization vector in current set; [-]
$\mathbf{y}$	Optimization vector in future set; [-]

Greek symbols

α_r	Ratio of wetted-area to total-volume fraction; [-]
ϵ	Effectiveness; [%]
η_p	Polytropic efficiency; [%]
π	Pressure ratio; [-]
σ_r	Ratio of flow-area to frontal-area fraction; [-]
τ	Torque; [N m]
φ	Form factor; [-]
χ	Solid-volume to total-volume fraction; [-]
Ω	Rotational speed; [rev/s]

Indices

0	Current best
1	Selection 1
2	Selection 2
AC	Aircraft
cold	Cold-side
con	Condenser
eng	Engine
fuse	Fuselage
fuel	Fuel
hot	Hot-side
i	Component index
inst	Installation
mat	Matrix
nac	Nacelle
ref	Reference
pl	Payload
vap	Vaporizer
wet	Wetted
$*$	Original aircraft

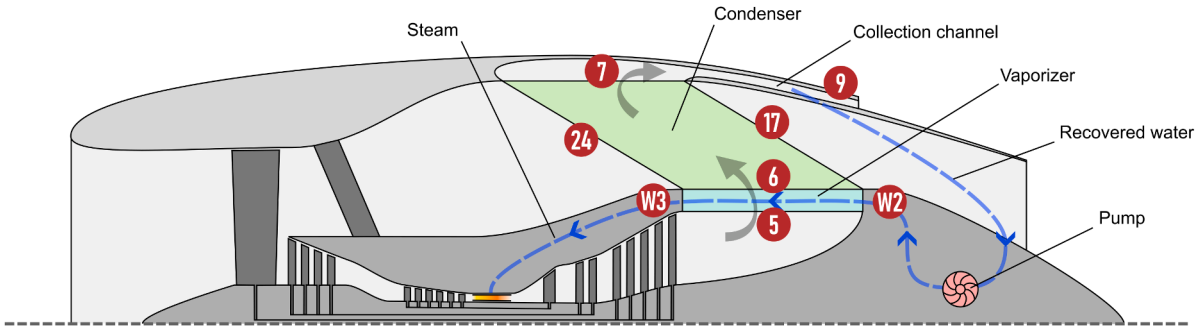

Fig. 1. Diagram of the Water Enhanced Turbofan (WET) engine, with important components and station numbers (red dots) marked. For a complete diagram of the station numbering, see Fig. A.1 for a conventional turbofan and Fig. B.1 for the WET engine. After the last turbine stage, the core air goes through, in order, the vaporizer (5-6), condenser (6-7), collection channel and the core nozzle placed in the aft end of the nacelle (7–9). The water recovered in the collection channel is drained to the core and pumped through the vaporizer (W2-W3) into the combustion chamber. (For interpretation of the references to colour in this figure legend, the reader is referred to the web version of this article.)

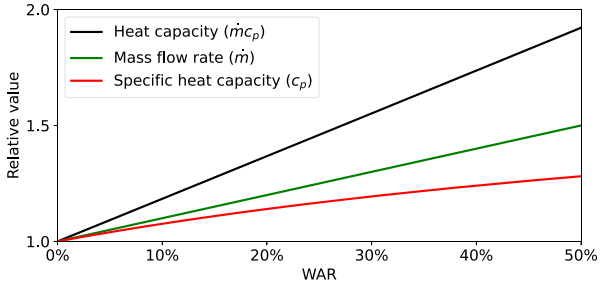

Fig. 2. The variation of heat capacity, mass flow rate and specific heat capacity in the core with varying water-air ratio (WAR). The values are taken at 700 K and 5 bar, with a fuel-air ratio (FAR) of 3%, and are given relative to no water injection.

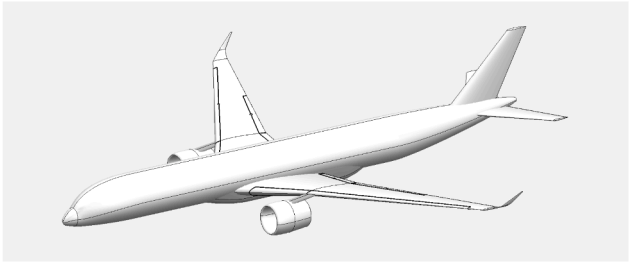

Fig. 3. Illustration of the Airbus A350-900 model generated in OpenVSP [16].

to the bypass flow, allowing water to be condensed out and recovered for recirculation.

The WET cycle increases efficiency through two thermodynamic effects. Firstly, by injecting water into the combustion chamber, the turbine mass flow is increased. Assuming the same combustion temperature, more power is generated, allowing for a larger fan, an increase in the bypass ratio (BPR) and the propulsive efficiency. This effect is amplified by the increased specific heat capacity that the added water introduces. Secondly, by heating the water before it is injected, using the core exhaust gas, the temperature of the core exhaust gas is cooled down. A cooler exhaust means less waste heat which increases thermal efficiency. The increase in thermodynamic efficiency due to water injection was demonstrated by Schmitz et al. for the WET cycle [6], and by Larson et al. [10] and Nishida et al. [11] for stationary power turbines.

Pouzolz et al. estimate that the thrust-specific fuel consumption (TSFC) can improve with 15–20% [12] as compared to an engine with entry into service in 2035. The reduced TSFC resulted in a fuel burn saving of 10–16% compared to the 2035 aircraft. Similar results were demonstrated in an engine cycle analysis performed by Kaiser et al. They achieved a TSFC decrease of 13% [13]. After installation effects, including the increased engine weight and nacelle drag, the fuel burn was reduced to 10%. A more recent study indicate that the benefit may be increased further by increasing overall pressure ratio (OPR) and turbine inlet temperature (TIT) [14]. Within that study constraints on the cycle were also identified including a limitation on the combustion chamber temperature at take-off and restrictions in the OPR due to the last-stage compressor blade height. The study did not include any design exploration or optimization of the heat exchangers, except to constrain the heat exchanger size to fit in the engine.

None of the studies discussed above [6,12–14] have provided sufficient detail to independently evaluate the benefits of the WET cycle. The studies use future engine reference cycles lacking some key data elements to be repeatable. Alternatively, they may compare one WET cycle concept against another to show further improvement. In Schmitz et al. [6] preliminary WET cycle data is presented in relation to a reference turboshaft engine. Only relative sizes are described and take-off performance is merely discussed not simulated. Furthermore, the paper uses the early concept of a fuselage integrated condenser. The work by Pouzolz et al. also use the earlier fuselage integrated condenser [12], and although fuel burn is presented for two mission lengths no details on the engine cycle are shared. For the work by Kaiser et al. [13] the more recent engine integrated condenser architecture is used, see Fig. 1, but the paper is not complete with respect to cycle detail. For instance, OPR is not stated for the WET cycle nor for the reference cycle. In Ziegler et al. [14], they also address the more recent condenser architecture, but the reported cycle improvements are given against another WET cycle.

As motivated by the previous discussion, there is a need for a paper that details the engine cycle and a corresponding reference cycle so that the work can be repeated independently. The current lack of data also means that it is difficult to repeat previous work with respect to heat exchanger performance, since the detailed assumptions on mass flow and sizing have not been presented fully. For the heat exchanger pressure loss, none of the main contributions on the WET cycle, i.e. [6,12–14], state pressure losses explicitly, despite that the cycle is very sensitive to this parameter. Our estimates presented herein indicate that close to half of the WET cycle performance benefits may be eroded solely by heat exchanger pressure loss. Although a weight distribution between main propulsion system groups is presented in Kaiser et al. [13], several cycle data are missing to allow comparing the results computed within this work. No OPR is given and the WAR is given only indirectly by relating it to the reference cycle fuel air ratio.

During take-off, the ambient temperature is higher than in cruise and hence the temperature difference for condensation is much lower. Thus, less water can then be extracted by the WET cycle in take-off. With less water injected, the heat capacity of the core stream decreases, see Fig. 2, due to the lower specific heat capacity of air compared to water. The lower heat capacity requires a higher temperature in the combustion chamber to keep the same power in the core flow. For example, if a cruise TIT of 1700 K is needed [13], we confirm a need for supplementary water as indicated by the original authors [6,13]. Although the authors do not state a take-off TIT, we observe a need for supplementary water even at a take-off TIT of 1950 K.

Herein, we present a detailed account of the WET cycle performance in relation to a reference engine including detail on pressure losses, weight distribution and nacelle drag estimates. We explore the design space of the WET cycle and evaluate its feasibility across different flight phases. The WET cycle specific components are modeled and combined with a model of a current state-of-the-art turbofan. Using the numerical model, the parameter space of the WET cycle is explored, including generalized heat exchanger design parameters [15], with the objective of reducing fuel burn during the cruise phase. This includes evaluating the installation effects of the engine and how this affects the aircraft design. The aim is to determine what performance benefits the WET concept has compared to a conventional turbofan. Furthermore, the cycle is evaluated at take-off to ensure that the cycle remains feasible during mission critical conditions, and can conform to the same requirements as the reference engine.

2. Theory

2.1. Reference engine and aircraft

The WET cycle is primarily intended for mid- to long-range missions, for which the aircraft consume a major part of their fuel at higher altitudes. The WET engine has been installed on a rubber-aircraft modeled around the Airbus A350-900 (A350) aircraft powered by the Trent XWB-84 engine, Fig. 3. The A350 is a modern twin-aisle jet airliner with a payload capacity of 53 300 kg, a maximum range of 8500 M and a maximum take-off weight (MTOW) of 283 000 kg. It can carry up to 440 passengers depending on the configuration.

The Trent XWB-84 is a high-performance, three-spool, high-bypass turbofan with cooling of the high- and intermediate-pressure turbines.

Table 1
Key cycle parameters for the Trent XWB-84 engine model evalated at cruise conditions. See Appendix A for further detail.

TIT	FPR	OPR	BPR	TSFC	Engine weight	Specific range
1650 K	1.58	47.1	8.99	14.97 mg N^{-1} s^{-1}	9526 kg	109.5 m kg^{-1}

Key cycle parameters are listed in Table 1. The tabulated data is supplemented by a more exhaustive listing of additional performance parameters in Appendix A. The intention of the listing in the Appendix is that the data set should be sufficient to allow repeating the cycle analysis. The performance model was derived using data from the ICAO emissions databank [17] and Jane's Aero engines [18]. Further information on the development of the XWB-84 engine model is found in Section 2.3.

The fan pressure ratio (FPR) and the interrelated bypass ratio (BPR) are important parameters for the cycle, as a lower FPR and specific thrust increases the propulsive efficiency of the engine. Their actual values are determined by optimization where lower FPR values are balanced out by increasing fan and low pressure turbine (LPT) weights [19] as well as through increased nacelle drag. In particular the rate of weight growth for the LPT with decreasing FPR becomes most difficult to manage in direct drive engines. The TIT has a large impact on the power available in the core stream and is coupled to the FPR and BPR by having to be sufficiently high to provide enough power to drive the fan. TIT is also higher during take-off conditions due to the increased ambient temperature, and it is important to consider constraints imposed by engine materials in this operating point. The OPR is related to the power usage, and is commonly set as high as possible in order to be able to extract as much energy as possible from the core flow. However, high OPR leads to a very small last stage of the high pressure compressor (HPC), which in turn leads to increased tip leakage losses, progressively reducing the benefit of a high pressure ratio. For the WET cycle, previous studies have suggested that OPR lower than typical is preferred in order to keep temperatures up for the WET cycle heat exchangers [13].

To quantify propulsion system performance, the TSFC, denoted by c_T, is often employed, relating thrust generation to fuel usage. Specific range, denoted by R_s, is a measure of aircraft efficiency quantifying how far the aircraft is able to fly given a kilogram of fuel. Specific range takes key aspects of integration into account, such as aircraft weight w_{AC} (in force terms), and the lift-drag ratio L/D, as indicated by Eq. (1). This equation also requires the speed of the aircraft V.

$$R_s = \frac{V \cdot L/D}{w_{AC} \cdot c_T} \tag{1}$$

To get a high specific range, a light aircraft with high lift-drag ratio and low TSFC is advantageous. Calculation of specific range requires an aircraft model. In this paper, a simplified model based on first order correlations was adopted. Specifically, the effect of engine weight on the structural weight and drag of the aircraft is of interest. The weight of the aircraft with changed engine weight is the sum of engine weight w_{eng}, the wing weight w_{wing} including the empennage after adjusting for heavier structures, the fuselage weight w_{fuse}, the fuel weight w_{fuel} and the payload weight w_{pl}, as described in Eq. (2).

$$w_{AC} = w_{eng} + w_{wing} + w_{fuse} + w_{fuel} + w_{pl} \tag{2}$$

Assuming constant wing loading, the reference area of the wing S_{wing} scales proportionally to the total weight of the aircraft, based on the reference wing area and weight of the original A350 (S^*_{wing} and w^*_{AC}, respectively) [20]. This relationship is described by Eq. (3).

$$S_{ref} = S^*_{ref} \cdot w_{AC}/w^*_{AC} \tag{3}$$

Resizing the wing adds additional structural weight, which is assumed to be proportional to the wing reference area, hence assuming a fixed thickness to chord for wing scaling. Since the only driver for aircraft weight increase is the engine weight, and the added engine weight only leads to a total aircraft weight increase of 4%, this assumption is deemed reasonable. Using the wing weight of the original A350 w^*_{wing}, this can be described as in Eq. (4).

$$w_{wing} = w^*_{wing} \cdot S_{ref}/S^*_{ref} \tag{4}$$

Combining Eqs. (3) and (4) into Eq. (2), we obtain

$$w_{AC} = \frac{w_{eng} + w_{fuse} + w_{fuel} + w_{pl}}{1 - w^*_{wing}/w^*_{AC}} \tag{5}$$

Assuming the same fuselage, fuel amount and payload, the engine weight alone determines the final aircraft weight. Resizing of the wing also changes the lift-drag ratio of the aircraft. For initial design estimations, Raymer [20] shows that the lift-drag ratio of a jet aircraft during cruise can be estimated using the aspect ratio A_r, the wetted area of the aircraft S_{wet}, the wing reference area and a constant $K_{L/D}$, according to Eq. (6). The main argument underpinning this correlation is that lift over drag needs to include not only the wing span and wing area, but also the total wetted area of the aircraft since this area relates directly to friction drag.

$$L/D|_{max} = K_{L/D} \cdot \sqrt{\frac{A_r}{S_{wet}/S_{ref}}} \tag{6}$$

Due to the limited space available between gates, airports are classified into different codes based on the maximum wing size that they can support. The A350 is at the upper limit for what an ICAO Code E airport can support, and for a resized aircraft to be able to fly the same routes to the same airports, it cannot increase in span. It is thus assumed that the span is fixed, and that an increase in wing area is accounted for by a larger chord. Assuming constant thickness-chord ratio, the wetted area of the wing increases proportionally to the chord. If the aircraft weight increases, the wetted area of the aircraft increases while the wing span remains the same, which leads to a lower lift-drag ratio.

A new engine design can also affect the diameter d and length l of the nacelle. The nacelle adds parasitic drag, which affects the thrust requirement of the engines and the aircraft fuel usage. The increase in nacelle drag due to increased diameter and length are taken into account by a method described by Raymer [20], in which the coefficient of drag for the nacelle $C_{D0,nac}$ is proportional to the wetted area of the nacelle, $S_{wet,nac}$ multiplied by a form factor. This is described in Eq. (7). The wetted area of the nacelle is roughly proportional to the length l times the diameter d. The form factor depends on the fineness ratio $\varphi = l/d$.

$$C_{D0,nac} \propto (1 + 0.35/\varphi) \cdot l \cdot d \tag{7}$$

The fineness ratio indicates that a thick and short nacelle will generate more drag than a thin and long nacelle, even if the surface areas are the same. The zero-lift drag coefficient was obtained through parasitic drag calculation in OpenVSP [21] using a model of the A350, and the induced drag coefficient was calculated using VSPAERO [21]. Wave drag is assumed to constitute 10% of the original total drag. The thrust requirement scales proportionally to the drag. Additionally, the increased diameter of the nacelle mandates special care when designing the wing. There needs to be enough clearance between the ground and the bottom of the nacelle. A significantly larger nacelle could require additional changes to the aircraft, such as mounting the engine on top of the wing, using a high-winged aircraft or extending the landing gears.

2.2. WET engine

The reference aircraft and engine were used as the design basis for the WET cycle concept. To derive the WET engine from the Trent XWB reference engine, the following architectural changes were made:

- Water injection was added to the combustion chamber.
- A vaporizer was placed after the last turbine stage.
- A condenser was placed after the vaporizer, using bypass air for cooling.
- A water collection channel was placed in the nacelle.

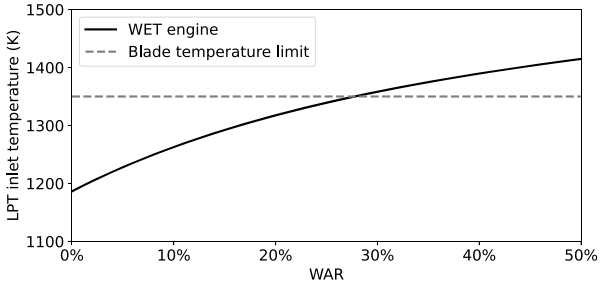

Fig. 4. Variation of the inlet temperature of the low pressure turbine (LPT) for the WET cycle during take-off, for fixed turbine inlet temperature (TIT) and overall pressure ratio (OPR). The blade temperature limit used is 1356 K, indicating a cooling need for several LPT stages.

- A pump was added to forward water from the condenser to the vaporizer.
- Cooling was added to the LPT, using air extracted from the HPC.

The WET cycle has a larger parameter space than the reference cycle due to the addition of the water loop and the heat exchangers. Most importantly, one needs to specify the water-air ratio (WAR) during cruise conditions. WAR affects the power available in the core as well as the heat transfer necessary to recover all injected water and close the water loop. The WET cycle also introduces two heat exchangers that need to be designed. As is shown in Section 2.4, this can be done on conceptual level by three additional non-dimensional parameters per heat exchanger. Proper care needs to be taken when selecting the heat exchanger parameters, as both the vaporizer and condenser affect the engine weight and size significantly [14].

Comparing to the reference engine, cooling of the LPT had to be added to the WET cycle as the increased heat capacity of the core flow with water injection leads to a slower reduction in temperature as the core flow expands through the turbines. The temperature at the LPT inlet is constrained by the maximum allowable blade temperature, which depends on the material choice, manufacturing process and coating type. Reviewing engine type certificates for recently introduced engines reveals that the LPT temperature may be as high as 1356 K [22], which in this work is assumed as an upper limit for having an uncooled LPT. Note that the LPT inlet temperature rises as the engine degrades. This increase results from the need to maintain the same thrust in take-off. The degradation forces a higher TIT, that in turn increases the LPT inlet temperature. Fig. 4 shows how the LPT inlet temperature of the WET engine changes with different levels of water injection during take-off. Here, we clearly see how the increased water content increases the LPT temperature. Notice that this effect gets stronger further down in the turbine expansion and at the LPT exit the XWB reference is more than 100 degrees colder than the WET cycle despite having the same take-off high pressure turbine inlet temperature. This is seen by comparing the take-off LPT exit temperature T_{05} for the reference engine and the WET engine as stated in Tables A.3 and B.5 respectively.

A tank was added for water storage. The water tank is a crucial components for the WET cycle [6,12,13], as some of the hotter conditions close to take-off will require supplementary water to be injected. To improve the aircraft performance while carrying such a system, advanced concepts may utilize mission points where it is possible to condense more water than needed to refill the tank. However, in this paper, all water required to perform a mission is assumed to be carried with the aircraft at take-off.

2.2.1. Limitations on WET cycle modeling

In a more advanced version of the WET cycle [13] steam turbines that extracts power from the vaporized water are introduced, supplying power to the low pressure shaft. The steam turbine increases the thermal efficiency of the cycle at a weight penalty. The magnitude of the benefits from the addition of the steam turbine are believed to be modest [13] and the component was not included in this analysis. Additionally, Kaiser et al. studies a cycle having two bypass streams: one hot flow that goes through the condenser and one cold flow that bypasses it. The benefit of reducing the amount of bypass air through the condenser is that it reduces the pressure losses incurred on the bypass air. Lower mass flow through the heat exchanger could also potentially reduce its size and help with diffusion upstream of the condenser. However, the condensation process is power intensive and requires large amounts of heat transfer. Furthermore, the temperature at which all of the injected water has condensed is close to the entry temperature of the air in the bypass channel. Together, these two effects greatly limit the potential for splitting the cooling flow into two streams, and therefore they are not studied in this work.

2.2.2. Combustion at high water-air ratio

Although water injection has been successfully demonstrated in the past, for instance on the JT3C-6 and the JT9D-3AW [23], the main target has then been to temporarily increase thrust rather than to continuously operate the combustor using water injection. Such an injection system only required successful implementation in a limited number of operating conditions at take-off rather than throughout a full flight envelope. This way of injecting water was also possible to integrate upstream of the combustor using spray bars, due to its much lower WAR requirement typically in the range of a few percent [23]. Other important efforts on integrating water injection has targeted NOx reductions [24]. Water rates of as much as 10% [25] have been demonstrated, but these systems have so far limited their commercial application to land based gas turbines. Even higher water air ratios have been explored experimentally using various fuels and superheated steam dilution reaching levels of 50% WAR [26,27]. These have shown reduced reaction kinetics due to the interaction of the steam in the combustion process.

The WET cycle relies on sustained water injection at unprecedented rates. Such systems are today at low technology readiness level. This work evaluates the potential of the WET engine concept, should future development of combustors be successful. It is noted that there is no need for a WET engine to inject all the water into the combustor directly, rather a major portion of the water may be injected downstream of the combustion zones [13]. This injection strategy could then be optimized to achieve good combustion stability, ignition characteristics, efficiency and durability over the entire operating range of the combustor.

2.3. Turbomachinery modeling

The thermodynamic cycle was modeled using turbomachinery relationships as described in Appendix A of Grönstedt [28] and implemented in the gas turbine performance code GESTPAN. Gas properties are interpolated from tables derived using the open-source NASA-developed Chemical Equilibrium with Applications (CEA) software [29]. For properties of pure water in both liquid and gaseous phase, the industrial formulations from the International Association for the Properties of Water and Steam were used [30–33]. The weight of the turbomachinery components was computed using the weight and cost estimation (WEICO) code, which is part of GESTPAN. WEICO follows the general procedure outlined by Tong et al. [34] where components are sized using empirical correlations, which allows for their weight to be estimated. WEICO has been developed and validated in multiple previous studies [35–37].

At the design point, the polytropic efficiency of the turbomachinery components, as well as the pressure ratios in the compressors are input. The same efficiency assumptions are made for the reference engine and the WET cycle. For off-design conditions, the efficiencies and pressure ratios are predicted based on the design values and interpolation from built-in compressor/turbine maps [28]. The compressors and turbines are connected using their rotational speed and torque. Electric power generation from the high pressure shaft for use in the avionics system and cabin systems is included. Bleed air from the HPC for environment

Table 2
Fixed heat exchanger parameters of the WET engine.

Parameter	Unit	Vaporizer	Condenser
t_W	mm	1.0	0.5
$l_f/\sqrt{t_f}$	$m^{1/2}$	0.33	0.33
ℓ	m	0.01	0.01
M_{hot}	–	0.1	–
M_{cold}	–	–	0.2
w_{inst}/w_{mat}	–	0.5	0.4
f/f_{ref}	–	0.75	0.75
j/j_{ref}	–	1.1	1.1
WRF	–	–	0.9

control in the cabin is also included. Cooling of the turbines is calculated stage-wise, for the stator and rotor separately [38].

To allow for an independent analysis of the results, extensive tables are provided in Appendices A and B. Tables A.1, A.3, B.2 and B.5 contain flow variables along the stations of the engine. Tables A.2, A.4, B.3 and B.6 contain variables pertinent to the operation of the turbomachinery components. Tables B.1, B.4 and B.7 contain heat exchanger design and performance variables. With these tabulations, it is be possible to reproduce the results presented in this work, using any commercially available gas turbine performance software, provided it allows for the incorporation of the WET cycle specific components.

2.4. Heat exchanger modeling

The WET concept requires two heat exchangers to be modeled, the condenser and the vaporizer. The heat transfer areas of these two units were modeled using the logarithmic mean temperature difference (LMTD) method. To be able to use the LMTD method, the overall heat transfer coefficient needs to be estimated. To evaluate the system performance, the pressure losses in each of the channels are important, as well as the weight of the heat exchangers. These parameters were modeled using the GenHEX method [15], where non-dimensional design parameters are used to estimate the heat transfer coefficient and the pressure loss for each channel. The GenHEX method has been developed through a number of publications [15,39], and has also been demonstrated for use in compact heat exchanger modeling for aircraft [40–43]. The benefit of the GenHEX method is the abstraction of design details and the generalizability towards different types of heat exchangers. The GenHEX method is used both during heat exchanger design and during off-design performance evaluation. The non-dimensional design parameters, also termed the generalized geometric parameters, are the ratio of wetted-area to total-volume fraction α_r, the ratio of flow-area to frontal-area fraction σ_r, and the solid-volume to total-volume fraction χ. By abstracting the heat exchanger using these parameters, various types of heat exchanger architectures can be evaluated without being explicitly selected, allowing a large number of concepts to be evaluated at an early design stage. The GenHEX correlation is derived from a database of heat exchanger performance data developed from Kay's and London's work [44]. This model only estimates the weight for the heat exchanger matrix and additional weight for its installation has therefore been modeled. The model excludes pressure losses due to diffusion in the ducts leading up to the heat exchangers. The GenHEX method also only estimates the matrix weight of the heat exchangers. Additional installation weight needs to be added, and this was assumed to be 50% and 40% of the matrix weight for the vaporizer and condenser respectively.

To fully define the parameters for the GenHEX method, three additional parameters need to be defined [15]. These are the wall thickness t_W, the characteristic length of the fins $l_f/\sqrt{t_f}$ and the undisturbed flow length ℓ. Their numeric values are listed in Table 2 together with the inlet Mach numbers used for the external sides of the two heat exchangers (M_{hot} and M_{cold}). For the condenser, the water recovery factor (WRF) also needs to be specified. The heat exchangers were assumed to be constructed from aluminum. To take into account uncertainty in the GenHEX method, as well as improvements to heat exchanger technology, the friction factor and Colburn factor were modified from the values estimated from the GenHEX method by a factor of f/f_{ref} and j/j_{ref}, respectively.

2.4.1. Vaporizer

The vaporizer is the first heat exchanger in the core flow path. It can be seen in Fig. 1, where stations 5 and 6 are the inlet and outlet of the core gas stream, respectively. Station W2 is the inlet of liquid water and station W3 is the outlet of superheated steam. The purpose of the vaporizer is to bring heat back from the core flow to the combustion chamber, while lowering the temperature of the hot core flow before it enters the condenser. It is often described as a combination of three different sections characterized by the state of the water: the economizer, evaporator and superheater. The division of the processes in the vaporizer simplifies the analysis and modeling of the component. It is assumed that all phase transition and no temperature change occurs in the evaporation section. The boiling of water causes a continuous change in the gas-to-liquid fraction, which makes it difficult to determine a single heat transfer coefficient for the whole evaporation section. Thus, the evaporator was discretized into smaller sections, in which the gas-to-liquid fraction was considered constant. For the mixture of liquid and gas phase, the heat transfer coefficient was calculated using relations for convective boiling flow in horizontal tubes, provided by the VDI Heat Atlas [45].

2.4.2. Condenser

The condenser is the second heat exchanger in the core flow path [46]. It can be seen in Fig. 1, where station 6 and 7 are the inlet and outlet of the core gas stream, respectively. Similarly, stations 24 and 17 are the inlet and outlet of bypass air. The purpose of the condenser is to cool down the core flow using the bypass air, until the water starts to condense out. The core gas flows radially outwards towards the nacelle, where the condensed water can be collected. The condenser is a cross-flow heat exchanger, and is modeled as a counter-flow heat exchanger with a correction factor developed by Jeter [47]. Like the vaporizer, the condenser can also be divided into multiple sections: an economizing and a condensing section. Since both temperature and phase changes occur simultaneously in the condensing section, the LMTD method cannot be applied directly. Instead, the condensing section is discretized into smaller sections, like the evaporator section in the vaporizer.

The air in the bypass channel has a high velocity, and it is important for the performance of the system to diffuse the bypass air flow before it reaches the condenser. The bypass air was diffused by tilting the heat exchanger forward in the channel and increasing the cross-sectional area of the flow path before the heat exchanger. It is important to target a small Mach number to minimize the pressure losses due to high flow velocities inside the heat exchanger. The heat exchanger was tilted 60° forward, which appeared to provide a good balance between sufficient diffusion and compactness.

Another important consideration for the condenser is the amount of water lost in the recovery process, commonly expressed using the Water Recovery Factor (WRF) mentioned earlier. It is the amount of recovered water over the total amount of water condensed. When the WRF is below 1, some of the condensed water is ejected through the core nozzle. It is thus necessary to condense some of the water produced from the combustion process, or water already present in the atmosphere, in order to recover as much water as was injected. It has been shown that, in order to keep down the size of the condenser, it is important to have a high WRF [46]. At the same time, it is currently difficult to estimate an appropriate value for the WRF. Throughout this report, a value of 0.9 has been used for the WRF, as noted in Table 2.

Table 3
Investigated cycle and heat exchanger parameters.

Parameter	Description	Cycle/component	Range
BPR	Bypass ratio		5–35
FPR	Fan pressure ratio		1.35-1.7
OPR	Overall pressure ratio	Cycle	20–50
TIT	Turbine inlet temperature		1650 K to 1850 K
WAR	Water-air ratio		10–50%
$\alpha_{r,vap}$	Surface density ratio		0.1–10
$\sigma_{r,vap}$	Void fraction ratio	Vaporizer	0.001-0.2
χ_{vap}	Compactness fraction		0.02-0.4
$\alpha_{r,con}$	Surface density ratio		0.01-0.3
$\sigma_{r,con}$	Void fraction ratio	Condenser	0.5–10
χ_{con}	Compactness fraction		0.01-0.06

3. Methodology

3.1. Parameter study and optimization

The cycle parameters selected for the parametric investigation are the WAR in the combustion chamber, BPR, FPR, OPR and TIT, as defined in Table 3. The cycle parameters are defined during typical cruise conditions, but vary for other mission points. During cruise, all of the injected water is assumed to be recovered, while during take-off, some of the injected water may come from the storage tank. The heat exchanger design parameters investigated are the ratio of wetted-area to total-volume fraction α_r, the ratio of flow-area to frontal-area fraction σ_r, and the solid-volume to total-volume fraction χ. Two sets of heat exchanger design parameters are required, one for the vaporizer and one for the condenser, which are designed differently to best support their specific flow conditions. The temperature to which the water is superheated in the vaporizer (the degree of superheating) can be varied based on a trade-off: a larger vaporizer will superheat the water more, recovering more power from the core flow, but will also increase the engine size and weight. In this paper, the degree of superheating was fixed close to the boiling point to simplify vaporizer sizing.

For a given WAR and TIT, the remaining cycle parameters and heat exchanger design parameters were optimized with respect to specific range, see Eq. (1). Although specific range does not capture the full variability seen during a mission profile, it scales approximately inversely to the total fuel burn of a mission. It is therefore used as a robust proxy for fuel burn, to allow for clear separation of contributions.

The initial optimization used the differential evolution algorithm [48], which is a stochastic optimization method. It works by iteratively perturbing an initial population towards an optimum. Differential evolution can handle problems where the objective function lacks a well-defined gradient and where the domain is discontinuous. The initial population was constructed using Sobol initialization [49], which is a randomized sampling technique designed to ensure more uniform coverage of the domain. Given a starting distribution of parameter vectors $\mathbf{x} \in \mathbb{R}^n$, and an objective function $f : \mathbb{R}^n \to \mathbb{R}$, each iteration generates a new set of vectors $\mathbf{y}$ from the current population $\mathbf{x}$, by modifying the components individually. For each component i, a random number $r_i \in [0, 1]$ is chosen. If $r_i > r_{\text{lim}}$, where $r_{\text{lim}} \in [0, 1]$ is a fixed optimization parameter, the component remains unchanged so that $y_i = x_i$. Otherwise, the component is modified according to Eq. (8), where $\mathbf{x}^0$ is the current best vector, $\mathbf{x}^1$ and $\mathbf{x}^2$ are randomly selected vectors from the current population, and F is a fixed optimization parameter.

$$y_i = x_i^0 + F \cdot \left(x_i^1 - x_i^2\right) \tag{8}$$

If $f(\mathbf{y}) < f(\mathbf{x})$, the vector $\mathbf{x}$ is replaced by $\mathbf{y}$ in the next population; otherwise, $\mathbf{x}$ is retained. The optimization was run until an adequate fitness was achieved. Thereafter, refinement was performed using the L-BFGS-B algorithm [50], a gradient based quasi-Newton method designed for efficient memory usage. The method approximates the inverse Hessian by storing only a small number of vector pairs containing past step updates and gradient differences, which are then used to form successive low-rank quasi-Newton updates.

All parameters were optimized simultaneously, due to the coupled nature of the cycle. Calculation of the engine performance during take-off was done to ensure full-mission feasibility by evaluating the required additional water to drive the cycle.

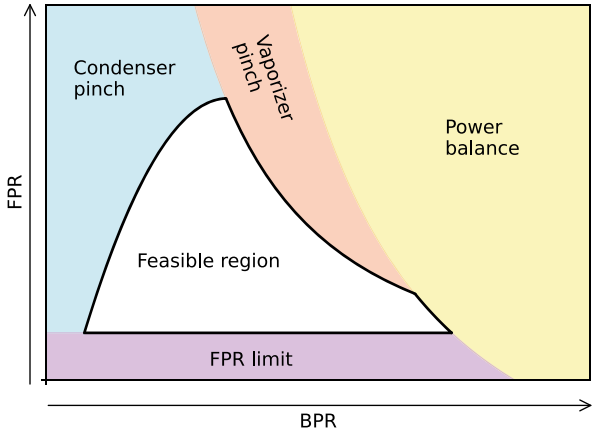

Fig. 5. Visualization of the main constraints (condenser pinch, vaporizer pinch, power balance and FPR limit) affecting the WET cycle, depicted in the bypass ratio (BPR) and fan pressure ratio (FPR) domain. The feasible region refers to where in the parameter space engines can be designed. The plot was constructed using a simplified thermodynamic model.

3.2. Thermodynamic constraints

It is important to find which sets of cycle parameters generate a feasible engine. Fig. 5 shows the main constraints that the cycle is under, as expressed in the BPR-FPR domain.

- **Condenser pinch.** The pinch point represents the point in the heat exchanger where the smallest temperature difference between the flow channels is encountered. When the temperature difference at the pinch point is zero, the heat transfer effectiveness becomes zero and no heat is transferred. Thus, a positive temperature difference is needed throughout the heat exchanger. For simplicity, the condenser temperature difference at the pinch point is assumed to be the same as for a counter-flow heat exchanger. Decreasing BPR reduces the heat capacity of the cold side of the condenser and thus the cooling capacity of the heat exchanger, leading to a lower limit on BPR. Although this is a cycle limitation, Section 4.1 shows that this constraint is not the main design driver as the region of high performance is not close to the constraint.
- **Vaporizer pinch.** The constraint on a positive temperature difference at the pinch point is likewise applicable for the vaporizer. Both FPR and BPR increase the specific power extracted from the core flow, which leads to lower core gas temperature after the turbines. The inlet temperature to the vaporizer needs to be sufficiently large in order to boil all the water before it is injected, which sets an upper bound to the FPR and BPR.
- **FPR limit.** To avoid having to use a variable fan nozzle and limit the heat exchanger size a lower FPR limit of 1.35 is assumed.
- **Power balance.** Similar to the vaporizer pinch constraint, the power balance constraint limits the amount of power that can be extracted from the core. For a fixed OPR, extraction of power from the core leads to a pressure drop across the turbines. This pressure drop, together with pressure losses incurred in the heat exchangers, determines the pressure at the core nozzle exit. The exit stagnation pressure needs to be kept above ambient.

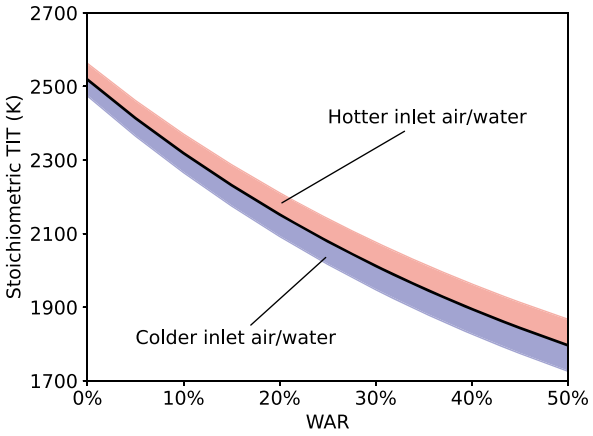

Fig. 6. Stoichiometric TIT versus WAR (black line) for a combustor inlet temperature of 700 K for both air and water. The lower light blue region indicates colder combustor inlet conditions (<700 K), and the upper pink region represents hotter combustor inlet conditions (>700 K). (For interpretation of the references to colour in this figure legend, the reader is referred to the web version of this article.)

Additionally, the engine needs to fulfill these and other requirements at all conditions that it might encounter during a mission. In particular, hot take-off conditions, with a deviation of 15 K from the International Standard Atmosphere (ISA), will be examined due to the high stress encountered during these conditions.

3.2.1. Cycle limit imposed by air dilution

The maximum amount of fuel that can be combusted is dependent on the amount of oxygen available. A stoichiometric fuel-air ratio (FAR) is the upper limit of fuel injection, and this coincides with the maximum TIT that can be reached. As WAR increases, the dilution increases and the temperature that can be reached is then reduced. The variation of maximum TIT with different levels of water injection is shown in Fig. 6. As the WAR increases, we see an expected trend of decreasing TIT. It is noteworthy that with the high levels of WAR discussed in this work as well as by previous authors, these conditions are quickly reached at take-off. For instance, a 50% WAR cycle restricts the maximum value of TIT below 1900 K, which is quite possible to exceed at take-off, as will be illustrated in Section 4. The two bands around the black line in Fig. 6 arise from variation in the compressor exit temperature driven by the selection of OPR and the temperature of the water as it enters the combustor.

4. Results and analysis

4.1. Thrust-specific fuel consumption in cruise

To investigate the basic relationships between the key design parameters we first map out TSFC and its dependence on BPR and FPR for a number of fixed values of WAR and TIT. This is done for optimal or near-optimal heat exchangers. After having analyzed the basic thermodynamic engine performance through the study of the TSFC values, we then extend the analysis to specific range as a function of aircraft and engine weight, nacelle drag and TSFC.

Sweeps of TSFC over FPR and BPR for multiple TIT and WAR can be seen in Fig. 7. The figures were generated by determining the optimal value of the remaining 9 variables in the 11-dimensional optimization space (Table 3). Converged values of the 9-dimensional parameter vector are established at the minimum TSFC point in each chart, but kept fixed for the BPR and FPR plotting. Looking at TIT of 1650 K and 30% WAR, the minimum TSFC is 13.68 mg N^{-1} s^{-1}. It appears that the region with the lowest TSFC is found close to the intersection between the FPR constraint and the vaporizer pinch constraint (alternatively the power balance constraint). As TIT increases, the feasible region expands towards higher BPR and FPR. The increase in TIT gives more available power in the core stream, which can be extracted in the LPT to power the fan. The LPT can thus support a larger fan or a fan with a higher pressure ratio. At the same time, the region where the lowest TSFC is found moves further towards higher BPR.

The most prominent trend in TSFC variation with WAR is that the optimal BPR increases. As the WAR increases specific power of the core flow increases which allows to drive a fan with a larger BPR. As seen from Fig. 5 the vaporizer pinch constraint limits further increase in BPR, because as more power is taken from the turbines the gas temperature at the LPT exhaust drops. Ultimately, the lowering of the LPT exhaust temperature will not allow heat exchange in the vaporizer. Increasing TIT has a beneficial influence on reducing TSFC, in particularly combined with high WAR values. The best TSFC is obtained for 40% WAR and TIT = 1850 K. It was attempted to perform a simulation also for 50% WAR and TIT 1850 K. However, as was discussed in the section cycle limit imposed by air dilution, even at stochiometric conditions a temperature of 1850 K temperature could be reached.

When optimizing the cycle parameters for TSFC, the BPR shows the expected behavior of increasing as the WAR increases. As the core increases its specific power it can drive a larger fan. At the same time, the FPR decreases. This indicates that BPR does not only increase with increasing water content due to the higher power available in the core, but also due to a trade-off with FPR. Looking at these parametric surveys an optimal WET cycle should be expected in the range 25–30 in BPR and with a matching FPR in the range 1.35-1.40. The WAR and TIT should both be relatively high, but a feasible solution must still exist. This means that both sufficient oxygen needs to remain to reach the sought TIT temperature despite the dilution with water, and that the take-off TIT does not become excessive. An WET cycle that maximizes the specific range will be presented in Section 4.3 below.

4.2. Take-off and need for additional water injection

At take-off, both the thrust requirement of the engine and the ambient temperature are at their highest. The high ambient temperature reduces the heat transfer capacity of the condenser, which means that the engine exhaust gas will leave the engine at a higher temperature. The saturated water content in this elevated temperature gas is substantially higher than at cruise and consequently less water may be returned to the cycle. In order to decrease the temperature to a reasonable level at take-off conditions, additional water from an onboard tank may therefore be required [6,13]. Injection of additional water increases the heat capacity of the core stream, allowing for a lower TIT while maintaining the power delivery across the turbines. The more additional water that is injected, the lower the TIT becomes for a given thrust setting. At the same time, the storage tank then adds additional weight to the system and requires a dedicated storage volume.

Fig. 8a displays the amount of additional water required at take-off to maintain a TIT of a maximum of 1850 K for a cruise WAR of 30%. As illustrated, the water flow depends on the thrust settings and ISA temperature deviation. As the ambient temperature increases (increasing deviation from ISA), the reduced condenser effectiveness decreases the amount of water that can be recovered, requiring additional water to be injected. It is important to consider how much additional water is required at the warmest condition that will be encountered, as the tank needs to be sufficiently large to supply enough water even during exceptionally warm days. From the figure, it can also be seen that the amount of water required increases with increased thrust demand. It is seen that for hot day (ISA + 15) take-off conditions, additional water in excess of 10 kg s^{-1} per engine, is required to keep the TIT down.

With increased WAR at cruise altitude, the effect of losing water at sea level becomes more significant as the engine components are designed for the corresponding water flow, and thus yet higher TIT are required to maintain thrust. At the same time, at high values of TIT

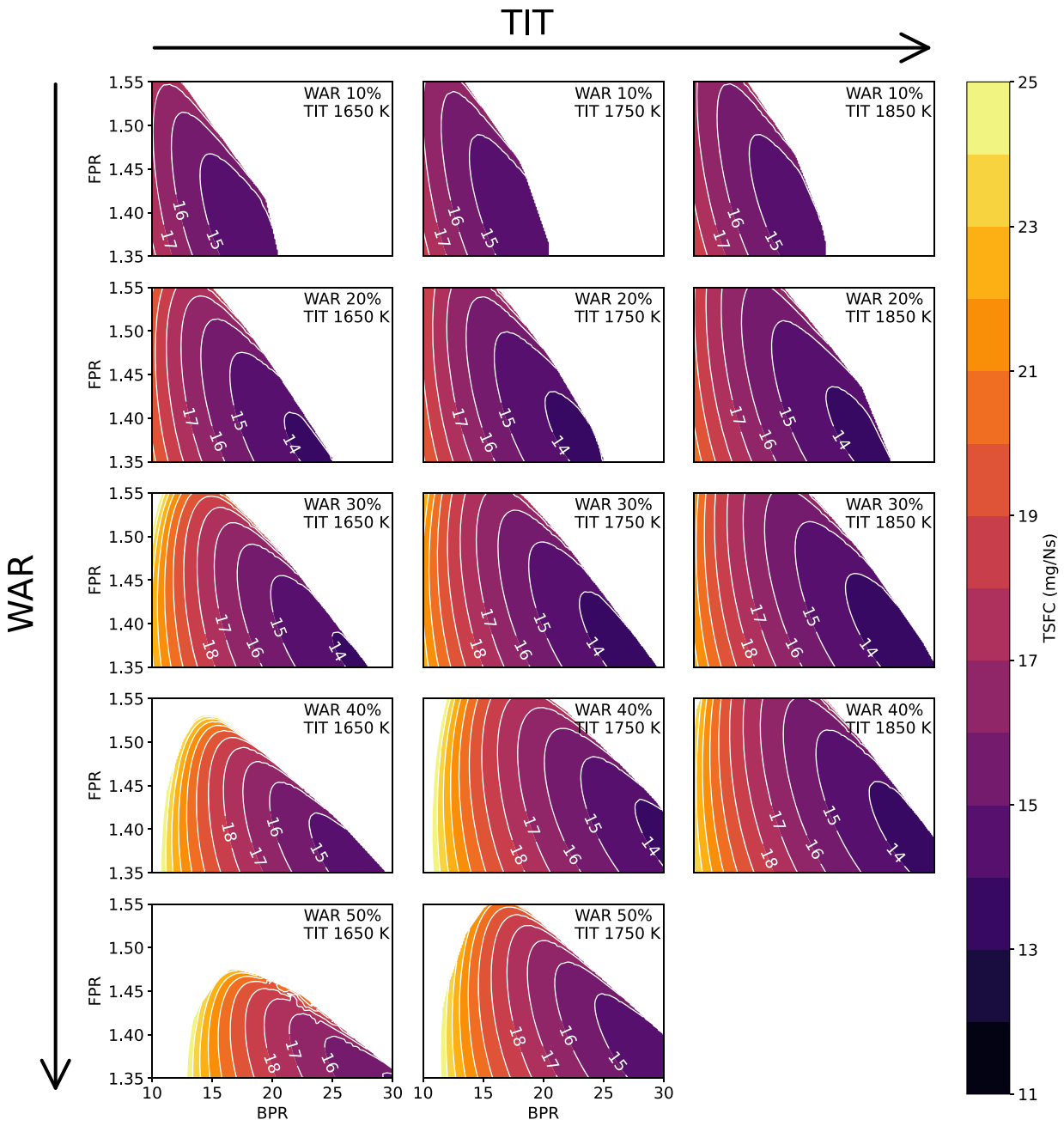

Fig. 7. Thrust-specific fuel consumption (TSFC) in cruise, for a variation of BPR and FPR. Each sub figure represents a selection of TIT, from 1650 K (left) to 1850 K (right), and WAR ranging from 10% (top) to 50% (bottom). The other cycle- and heat exchanger parameters were set by determining suboptimal values for specific range. No map is presented for a TIT of 1850 K and 50% WAR as it is not possible to reach that temperature with that amount of water.

in cruise, the additional water might be insufficient to cool the combustion chamber at take-off. Fig. 8b displays the minimum amount of water required to keep the combustion chamber temperature below 1950 K at take-off, for a range of WAR and TIT during cruise. At high design WAR, it is not possible to achieve a combustion chamber temperature below 1950 K, no matter how much additional water is added. This was the case for all engines with a design WAR of 50%. The same is true for low design WAR and high TIT. Furthermore, the lower the cruise TIT and WAR, the less additional water is required to cool the engine at take-off.

The main conditions that require additional water are the take-off phase and the initial part of the climb phase. During loiter, some water is also required to keep the water cycle running in case a sudden thrust increase requirement. Additionally, the aircraft needs to be able to perform a diversion mission in case it is impossible to land at the intended airport. As with fuel, a certain amount of water should be provided as reserve in case of contingencies. The water that will be used after the cruise phase, including the reserve, will either be carried with the aircraft through the cruise phase, increasing the weight and the fuel burn, or it will be extracted during the cruise phase by over-dimensioning the condenser. An approximate division of the stages of flight that require additional water, including their duration and the estimated total amount of water required, can be seen in Table 4. The estimate is done for 30% WAR and a TIT of 1850 K, and during a hot day (ISA + 15). In total, 10.4 m^3 of water is required. The water consumption for initial climb, loiter and diversion climb are estimated from the take-off water consumption based on ambient temperature and thrust setting. The

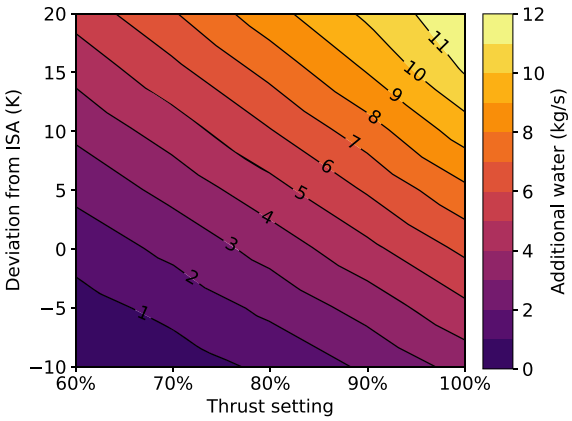

(a) Additional water needed to maintain take-off TIT at 1850 K for 30% WAR with varying thrust and deviations from International Standard Atmosphere (ISA) conditions.

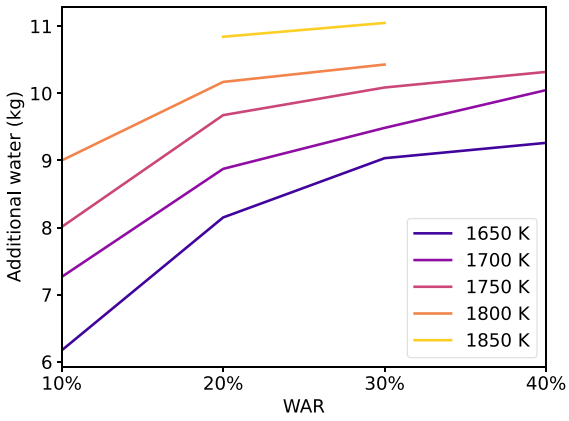

(b) Additional water needed to maintain take-off TIT below 1950 K for a range of cruise TIT designs.

Fig. 8. Comparison of water injection requirements at take-off for a single engine.

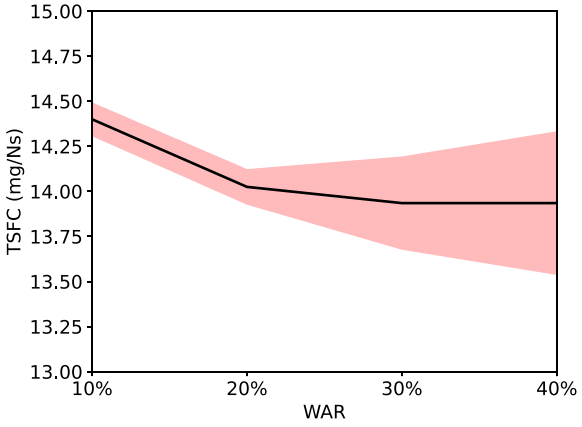

(a) TSFC

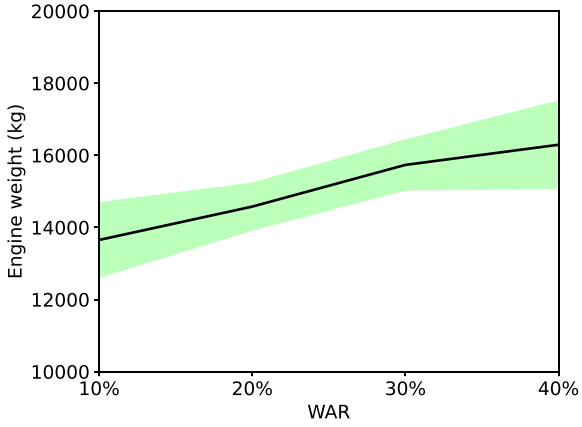

(b) Engine weight

Fig. 9. Optimized WET engine trends in cruise for TSFC and single-engine weight.

Table 4
Water usage for the WET cycle engine with an engine designed for 30% WAR and TIT of 1850 K. A 10% reserve is assumed.

Phase	Consumption (kg s^{-1})	Duration (min)	Load (kg)
Take-off	22.0	2	2640
Initial climb	9.4	5	2820
Loiter	2.0	10	1200
Diversion climb	9.4	5	2820
Reserve	–	–	948
Total	–	–	10,428

tank is estimated to weigh 1566 kg. An optimistic approach is taken for calculating the specific range, wherein the water tank is assumed to be replenished during cruise. Thus, tank weight is included in the estimation of specific range during cruise, while the water weight is neglected.

4.3. Weight, drag and specific range

A sequence of optimizations for different WAR have been conducted in the cruise condition. The resulting TSFC for these optimizations can be seen in Fig. 9a, together with the single-engine weight in Fig. 9b. Notice that since the optimum value of these parameters is influenced by other parameters there is a spread in the optimized value when plotted only upon WAR. Still, quite clear trends with WAR can be seen. For all the examined engines, a cruise TSFC lower than for the reference engine was observed. The lowest TSFC achieved was 13.54 mg N^{-1} s^{-1}, which is 9.6% lower than for the reference engine, achieved at 40% WAR with a TIT of 1750 K. As will be demonstrated in Section 4.4 the potential cycle efficiency benefit of the WET engine is estimated at around 20%, but the impact of the heat exchanger pressure loss is estimated to approximately halve these benefits. Thus, it is clear that a more optimistic heat exchanger modeling would easily have matched the 13% reduction in TSFC reported in [13]. As seen in Fig. 9b there is also a clear growing trend in engine weight with increasing WAR, suggesting a diminishing return as WAR increases.

As discussed, the influence of the weight and drag of the aircraft needs to be modeled as well to make it possible to predict the specific range, defined by Eq. (1). For the WET engine, we add two extra heat exchangers, which are expected to increase the engine weight. Furthermore, as discussed in Section 2.1, increased engine weight affects the structural weight and drag of the aircraft wing. The WET engine also requires a larger nacelle diameter to accommodate adequate diffusion before the condensing heat exchanger, as well as a longer na-

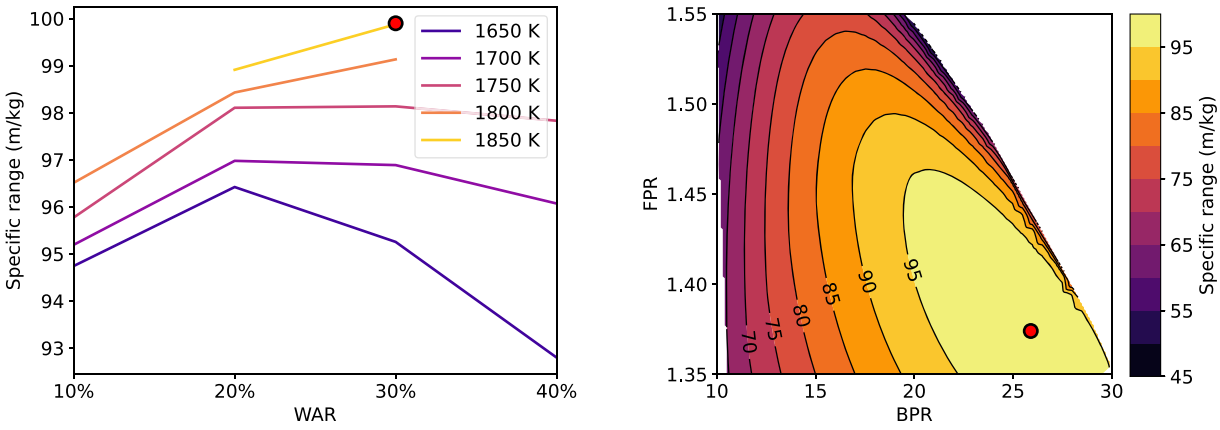

(a) Trends in specific range for a variation in WAR, for TIT between 1650 K and 1850 K. Engines for which no feasible parameter configuration was found have been excluded.

(b) Specific range over BPR and FPR for TIT of 1850 K and 30% WAR.

Fig. 10. Comparison of specific range of optimized engines. The red dot represents the optimized WET cycle presented in Table 5. (For interpretation of the references to colour in this figure legend, the reader is referred to the web version of this article.)

celle to make room for both heat exchangers. A larger nacelle increases parasitic drag. Combined, these two effects contribute to the increased thrust that the engine is required to produce. As is seen in Fig. 9b, the engine weight for all the optimized engines is significantly larger than for the reference engine, which only weighs 9526 kg. The higher the WAR, the heavier the engine becomes due to the increased weight of the heat exchangers.

The computed optimum specific range with WAR is shown in Fig. 10a, while Fig. 10b presents a sweep in BPR and FPR for the best-performing engine. It is clear that for high TIT, increased WAR allows for increased specific range despite the weight and drag penalties incurred from heavier heat exchangers. For lower TIT, increasing WAR beyond 20% is detrimental to specific range. At higher WAR TIT impacts the performance of the cycle significantly. Dropping TIT from 1850 K to 1650 K at 30% WAR results in a decrease in specific range of 4.6%. We also observe a strong similarity between the contours of specific range in the BPR and FPR domain as seen for the previously discussed contours of TSFC in Fig. 7, except for a slight shift towards lower BPR and higher FPR.

The best performance was achieved at 30% WAR, for which the highest specific range was 99.9 $\mathrm{m\,kg^{-1}}$. This is still 8.8% lower than for the Trent XWB reference engine. As will be discussed in next section, using more optimistic assumptions on the nacelle drag and heat exchange pressure loss it may be possible to reach the performance of the reference cycle.

A comparison between the reference engine and the best performing WET engine can be seen in Table 5. The lower TSFC in the WET cycle is in part due to the lower FPR compared to the reference, which increases the diameter of the fan. This trade can be made for a conventional engine as well at the cost of increased nacelle diameter. However, since the nacelle diameter of the WET engine is set by the size of the condenser, the penalty for increasing the fan diameter is removed. Although the TSFC is lower for the WET cycle than for the reference cycle, the increased weight and drag caused by the heat exchangers resulted in overall performance losses. The TIT during cruise is significantly elevated for the WET engine. Normally, these temperatures are only reached for short periods where high performance is needed. The extended period of time that the engine has to work at elevated temperatures will likely reduce the life of the combustion chamber and turbine components. The FAR is also significantly higher for the WET engine than for the reference engine, and it approaches stoichiometric conditions at take-off. The inlet temperature of the LPT is elevated beyond the blade temperature limit of 1350 K for the take-off phase, even without accounting for engine degradation, which indicates that LPT cooling would be needed.

Table 5
Comparison between the Trent XWB reference engine and the WET engine with 30% WAR and a cruise TIT of 1850 K.

		Ref.		WET	
Parameter	Unit	Cruise	T/O	Cruise	T/O
Altitude	m	10,668	1524	10,668	1524
Mach no.	–	0.84	0.20	0.84	0.20
Deviation from ISA	K	0	15	0	15
Mass flow air	$\mathrm{kg\,s^{-1}}$	619	1312	888	1745
TSFC	$\mathrm{mg\,N^{-1}\,s^{-1}}$	14.97	9.85	13.71	8.47
Specific range	$\mathrm{m\,kg^{-1}}$	109.5	–	99.9	–
BPR	–	8.99	8.56	25.89	23.65
OPR	–	47.1	50.6	45.8	49.0
FPR	–	1.576	1.624	1.374	1.406
TIT	K	1650	1945	1850	1952
FAR	%	2.54	3.15	5.75	6.82
WAR	%	–	–	30.0	39.1
Fan diameter	m	3.000	3.000	3.595	3.595
Nacelle diameter	m	3.751	3.751	5.257	5.257
Nacelle length	m	5.493	5.493	6.706	6.706
Engine weight	kg	9526	9526	15,825	15,825
Vap. volume	$\mathrm{m^3}$	–	–	0.600	0.600
Con. volume	$\mathrm{m^3}$	–	–	22.77	22.77
LPT inlet temperature	K	993.4	1187.8	1239.4	1363.3
LPT outlet temperature	K	665.3	816.6	795.7	911.3
Vap. inlet temperature (hot)	K	–	–	795.7	911.3
Vap. inlet temperature (cold)	K	–	–	291.0	347.0
Vap. outlet temperature (hot)	K	–	–	457.8	551.9
Vap. outlet temperature (cold)	K	–	–	573.6	587.8
Con. inlet temperature (hot)	K	–	–	457.8	551.9
Con. inlet temperature (cold)	K	–	–	269.2	320.7
Con. outlet temperature (hot)	K	–	–	291.0	347.0
Con. outlet temperature (cold)	K	–	–	301.6	348.6
Vap. pressure loss (hot)	%	–	–	2.7	1.9
Vap. pressure loss (cold)	%	–	–	0.0	0.0
Con. pressure loss (hot)	%	–	–	14.9	8.5
Con. pressure loss (cold)	%	–	–	2.9	2.7
Vap. effectiveness	%	–	–	67.0	63.7
Con. effectiveness	%	–	–	91.5	91.6

The distribution of component weights for the best performing WET engine can be seen in Fig. 11. The heat exchangers increase the engine

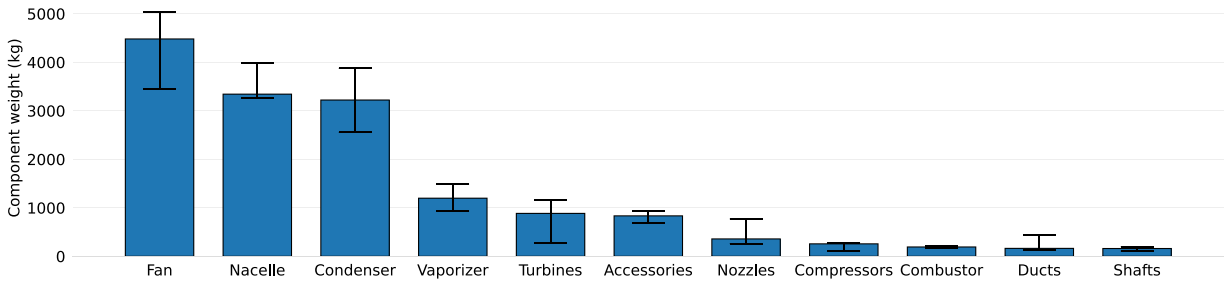

Fig. 11. Component weight distribution for the WET engine, with TIT of 1850 K and 30% WAR. The error bars represent the 95% confidence interval and were generated by varying structural design parameters within WEICO in a Monte Carlo simulation.

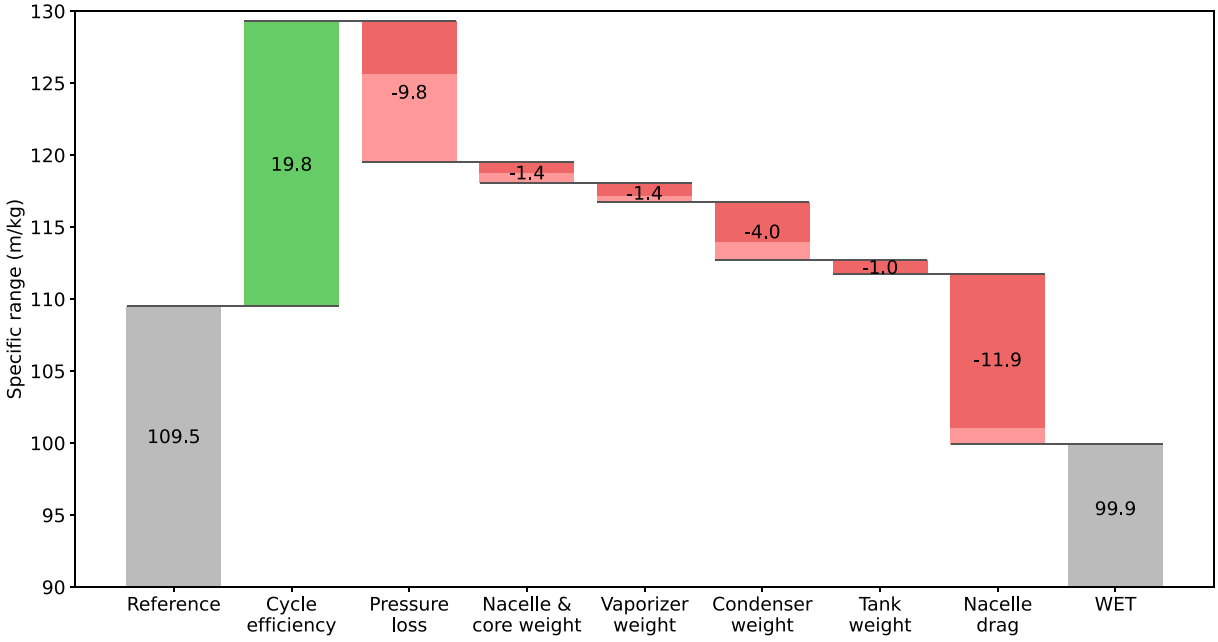

Fig. 12. Waterfall chart of the influence of different factors on specific range, presented for 30% WAR and TIT of 1850 K. Green and red bars indicate an increase and decrease in specific range, respectively. The pink portion of the red bars indicate how much of the losses can be removed by assuming Chilton-Colburn optimal heat exchangers, as described in Section 4.4. (For interpretation of the references to colour in this figure legend, the reader is referred to the web version of this article.)

weight significantly, and make up approximately a third of the total engine weight. Although the vaporizer is significantly smaller in volume than the condenser, it still weighs approximately 37% of the condenser due to its higher compactness.

Despite the higher thermodynamic efficiency of the wet cycle compared to a conventional turbofan cycle, the WET engine exhibits lower specific range than the Trent XWB reference engine. A waterfall chart depicting the main factors affecting the specific range of the WET engine can be seen in Fig. 12. The effects can be divided into four parts: The cycle efficiency, the heat exchanger pressure losses, different component weights and the nacelle drag. The large improvement in cycle efficiency is caused by the return of heat from the core flow to the combustion chamber via the vaporizer and water injection. The specific range gain due to efficiency improvement is however halved when considering the pressure losses encountered in the two heat exchangers. Note that pressure losses are only modeled for the flow in the heat exchanger matrix, the pressure losses caused in the installation ducts are not accounted for suggesting that the modeling is still on the optimistic side. The weight of the heat exchangers, as well as an increased weight of the other engine components and the addition of the water tank, reduces the specific range by a similar amount. The largest reduction, however, comes from the greatly increased nacelle drag. The nacelle size increased mainly due to the condenser, which accounts for approximately 97% of the total heat exchanger volume. The large difference in heat exchanger volume results primarily from the fact that the condenser internal flow is comprised of the whole core flow whereas the internal flow of the vaporizer is sized to accommodate the recirculated water. Additionally, the condenser passes all the bypass flow through its external side whereas the vaporizer passes only the core flow over its external surface. The nacelle drag was not accounted for in some of the previous studies [14,46], but was recently included in the work by Kaiser et al. [13], and to a limited degree in the work by Pouzolz et al. [12].

4.4. Specific range improvement potential

Accurate heat transfer models are crucial for determining the performance benefits of the cycle. The GenHEX model uses correlations based on real-world heat exchangers to estimate performance parameters. The correlations for Colburn factor and friction factor are found to be within ±25% for 94% and 69% of heat exchangers, respectively, when compared to real heat exchangers [15]. This introduces uncertainty in the estimation of pressure loss and heat transfer, which affects the resulting specific range. Furthermore, future heat exchangers could potentially provide better performance than existing heat exchangers.

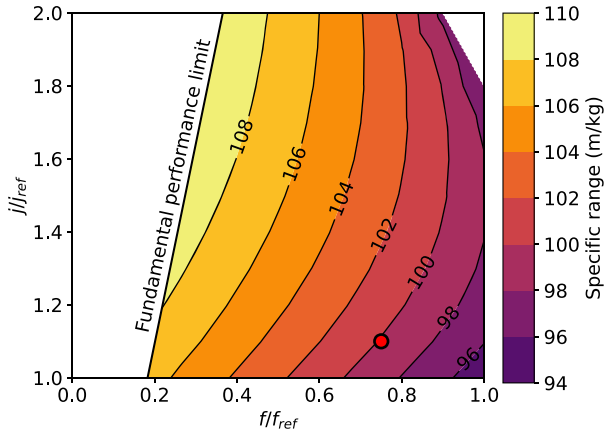

Fig. 13. Specific range under variation of Colburn factor (j) and friction factor (f), for 30% WAR and a TIT of 1850 K. The red dot represents the assumption used in this report. The white region to the left of the fundamental performance limit, is infeasible with respect to the Chilton-Colburn J-factor analogy. The reference value for Colburn factor (j_{ref}) and friction factor (f_{ref}) were obtained using the GenHEX method [15]. (For interpretation of the references to colour in this figure legend, the reader is referred to the web version of this article.)

Considering the strong impact that heat exchanger pressure losses and size have on the cycle performance, it is important to evaluate the effect that correlation uncertainty has on the performance. The friction and Colburn factors were decreased and increased, respectively, to emulate heat exchangers with improved performance. The results are mapped out in Fig. 13 for the best performing case with 30% WAR and a TIT of 1850 K.

There is a fundamental limit to the performance that can be achieved, as a certain amount of pressure loss is needed in order to facilitate heat transfer through forced convection. This is commonly described by the Chilton-Colburn J-factor analogy [51]. The white region in Fig. 13 represents parameter combinations surpassing this fundamental limit, and is thus not of interest as no technology can reach it. In Fig. 12 we have illustrated the performance benefits that can be obtained if the Chilton-Colburn performance bound is reached. The losses that can be removed are indicated as light red whereas the losses that remain even at the Chilton-Colburn limit are marked as darker red. Notice that the advanced heat exchanger technology has a beneficial impact not only on pressure loss, but as heat transfer increases the heat exchanger gets more compact allowing nacelle drag to be reduced and condenser and vaporized weight is reduced simultaneously. To attain the limit, the currently assumed Colburn coefficient needs to be increased by 80% and the friction coefficient needs to be reduced by 67%. This is a very optimistic scenario, since the current values represent an average value of existing heat exchangers [15]. Then, the TSFC decreases to 13.04 $\text{mg N}^{-1}\,\text{s}^{-1}$, which is 12.9% lower than the Trent XWB reference engine. If this limit could still be attained, an increase in specific range to 109.5 m kg^{-1} would be achieved, which happens to be the same performance as noted for the reference aircraft. Thus, even under optimistic heat exchanger technology assumptions, no improvement in net specific range appears to be achievable.

5. Conclusions

A performance analysis of the WET cycle has been performed covering key cycle parameters (WAR, TIT, FPR, BPR, OPR) as well as key heat exchanger parameters. Comparing the optimal WET cycle engine with the reference XWB engine, a 9.6% reduction in TSFC was achieved at 40% WAR and TIT of 1750 K. However, including the increased propulsion system size and weight needed to accommodate the heat exchanger components, no fuel burn reduction could be achieved. This conclusion was robust over a wide range of heat exchanger performance parameter variations, with the WET cycle only reaching the reference engine performance when assuming that the heat exchangers would run at the Chilton-Colburn performance bound.

Since the water recovery capability of the WET cycle depends on the temperature in the bypass channel, more water is rejected to the ambient at take-off. Therefore, the amount of recovered water will inevitably be lower at take-off than in cruise. This causes a reduction in the specific power for the core. In turn, to achieve the required engine thrust the TIT at take-off will have to be increased in order to compensate for the lack of water. For this reason, the cycles with the highest cruise WAR and TIT will either have to use a large amount of supplementary water at take-off or they become infeasible due to excessive TIT. Unfortunately, these high WAR and TIT cycles also show the largest benefits in cruise TSFC, meaning that the best WET engine cycles will be compromised by large supplementary water needs in take-off. In association with this, we also highlight the challenges with cooling the WET cycle. The high specific power of the higher WAR cycles causes the temperature to drop off at a lower rate as the pressure decreases through the turbines. With high TIT cycles this leads to unusually high temperatures in the later parts of the expansion, meaning that the LPT may need cooling. Alternatively, some cruise TSFC needs to be traded for a lower take-off TIT to drop the temperature throughout the turbine expansion.

CRediT authorship contribution statement

Filip Herbertsson: Writing – original draft, Visualization, Software, Methodology, Data curation; **Xin Zhao:** Software; **Anders Lundbladh:** Writing – review & editing; **Tomas Grönstedt:** Writing – original draft, Supervision, Funding acquisition, Conceptualization.

Data availability

Data will be made available on request.

Declaration of competing interest

The authors declare that they have no known competing financial interests or personal relationships that could have appeared to influence the work reported in this paper.

Funding sources

This work was supported by the Swedish Energy Agency [grant number P2023-01514].

Appendix A. Performance of the Trent XWB reference engine

A.1. Station numbering for the Trent XWB reference engine

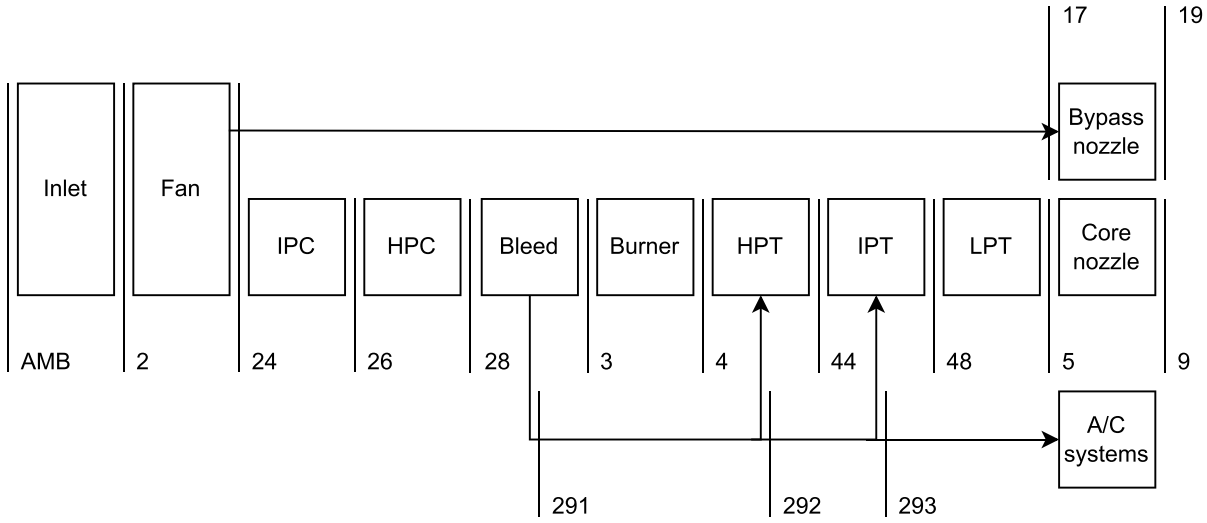

Fig. A.1. Station numbering for the Trent XWB-84 engine, based on the "SAE Aerospace Recommended Practice 755 - Turbine Engine Performance Station Numbering".

A.2. Cruise performance of the XWB engine

Table A.1
Flow variables of the Trent XWB reference engine model during typical cruise conditions.

Station	p_0 (bar)	T_0 (K)	$\dot{m}$ (kg s^{-1})	FAR
AMB	0.238	218.8	618.68	0.0000
2	0.379	249.8	618.68	0.0000
24	0.552	281.0	61.95	0.0000
26	4.692	545.8	61.95	0.0000
28	17.832	805.9	61.95	0.0000
291	17.832	805.9	16.92	0.0000
292	17.832	805.9	4.51	0.0000
293	17.832	805.9	0.84	0.0000
3	17.832	805.9	45.03	0.0000
4	17.023	1650.0	46.18	0.0254
44	7.188	1260.7	58.59	0.0199
48	2.778	993.4	62.26	0.0187
5	0.498	665.3	62.26	0.0187
9	0.489	665.3	62.26	0.0187
17	0.597	287.4	556.73	0.0000
19	0.589	287.4	556.73	0.0000

Table A.2
Turbomachinery variables of the Trent XWB reference engine model during typical cruise conditions.

Parameter	Unit	Fan	IPC	HPC	HPT	IPT	LPT
$\dot{W}$	MW	23.201	16.709	15.993	15.993	16.709	23.201
π	–	1.5757	8.5029	3.8008	2.3681	2.5875	5.5834
η_p	–	0.9270	0.9063	0.9205	0.8960	0.9109	0.9196
τ	N m	130,326	22,468	14,936	14,936	22,468	130,326
Ω	rev/s	28.33	118.36	170.41	170.41	118.36	28.33
A	m^2	6.7048	0.6238	0.1028	0.0281	0.0734	0.1782

A.3. Take-off performance of the XWB engine

Table A.3
Flow variables of the Trent XWB reference engine model during hot day take-off conditions.

Station	p_0 (bar)	T_0 (K)	$\dot{m}$ (kg s^{-1})	FAR
AMB	0.843	293.2	1311.50	0.0000
2	0.867	295.6	1311.50	0.0000
24	1.302	335.1	137.24	0.0000
26	11.442	651.1	137.24	0.0000
28	43.847	954.3	137.24	0.0000
291	43.847	954.3	36.10	0.0000
292	43.847	954.3	8.23	0.0000
293	43.847	954.3	0.00	0.0000
3	43.847	954.3	101.13	0.0000
4	41.882	1945.2	104.32	0.0315
44	17.736	1497.0	132.19	0.0247
48	6.881	1187.8	140.42	0.0232
5	1.307	816.6	140.42	0.0232
9	1.287	816.6	140.42	0.0232
17	1.408	342.7	1174.27	0.0000
19	1.391	342.7	1174.27	0.0000

Table A.4
Turbomachinery variables of the Trent XWB reference engine during hot day take-off conditions.

Parameter	Unit	Fan	IPC	HPC	HPT	IPT	LPT
$\dot{W}$	MW	61.672	44.743	43.021	43.021	44.743	61.672
π	–	1.6241	8.7855	3.8322	2.3614	2.5775	5.2632
η_p	–	0.9365	0.9082	0.9204	0.8963	0.9108	0.9266
τ	N m	314,982	54,063	36,852	36,852	54,063	314,982
Ω	rev/s	31.16	131.72	185.79	185.79	131.72	31.16
A	m^2	6.7048	0.6238	0.1028	0.0281	0.0734	0.1782

Appendix B. Performance of the WET engine

B.1. Station numbering for the WET engine

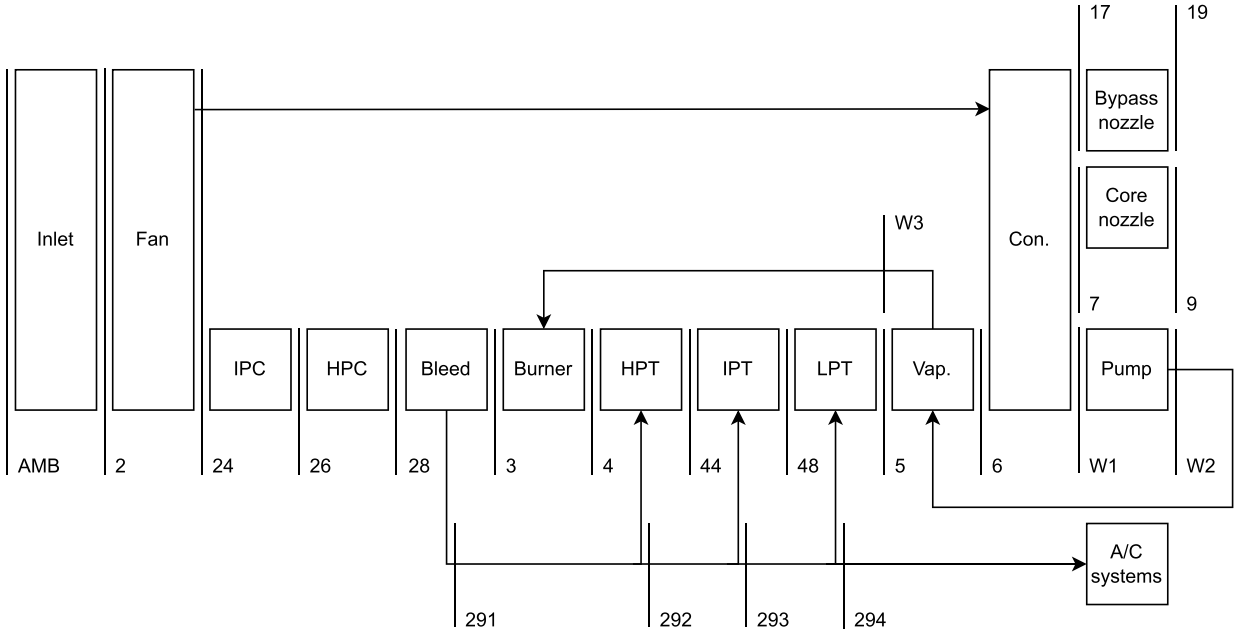

Fig. B.1. Station numbering for the WET engine, based on the "SAE aerospace recommended practice 755 turbine engine performance station numbering".

Table B.1
Heat exchanger geometric parameters of the optimized WET engine.

Parameter	Unit	Vaporizer	Condenser
α_r	–	1.410	0.067
σ_r	–	0.188	2.535
χ	–	0.2888	0.0246
t_W	mm	2.0	0.5
$l_f/\sqrt{t_f}$	$m^{1/2}$	0.33	0.33
ℓ	m	0.01	0.01
A_{hot}	m^2	5.26	11.34
A_{cold}	m^2	5.26	28.62
L_{hot}	m	0.373	3.062
L_{cold}	m	0.373	1.213
M_{hot}	–	0.1	0.0578
M_{cold}	–	0.0037	0.2
WRF	–	–	0.9
w	kg	1814	2541

B.2. Cruise performance of the WET engine

Table B.2
Flow variables of the optimized WET engine during typical cruise conditions.

Station	p_0 (bar)	T_0 (K)	$\dot{m}$ (kg s^{-1})	FAR	WAR
AMB	0.238	218.8	888.18	0.0000	0.000
2	0.379	249.8	888.18	0.0000	0.000
24	0.481	269.2	33.04	0.0000	0.000
26	4.319	532.3	33.04	0.0000	0.000
28	17.335	799.3	33.04	0.0000	0.000
291	17.335	799.3	14.79	0.0000	0.000
292	17.335	799.3	3.77	0.0000	0.000
293	17.335	799.3	1.68	0.0000	0.000
294	17.335	799.3	0.84	0.0000	0.000
3	17.335	799.3	18.25	0.0000	0.000
4	16.548	1850.0	24.77	0.0575	0.300
44	8.222	1427.9	35.79	0.0358	0.187
48	4.359	1239.4	37.88	0.0335	0.175
5	0.542	795.7	38.72	0.0326	0.170
6	0.528	457.8	38.72	0.0326	0.170
7	0.449	291.0	33.25	0.0326	0.000
9	0.441	291.0	33.25	0.0326	0.000
17	0.505	301.6	855.14	0.0000	0.000
19	0.499	301.6	855.14	0.0000	0.000
W1	0.449	291.0	5.47	–	–
W2	17.335	291.0	5.47	–	–
W3	17.335	573.6	5.47	–	–

Table B.3
Turbomachinery variables of the optimized WET engine during typical cruise conditions.

Parameter	Unit	Fan	IPC	HPC	HPT	IPT	LPT
$\dot{W}$	MW	22.935	8.838	9.179	9.179	8.838	22.935
π	–	1.3738	8.9786	4.0134	2.0127	1.8863	8.0375
η_p	–	0.9270	0.9063	0.9205	0.8987	0.9146	0.9178
τ	N m	128,833	11,885	8572	8572	11,885	128,833
Ω	rev/s	28.33	118.36	170.41	170.41	118.36	28.33
A	m^2	9.6261	0.3735	0.0588	0.0177	0.0451	0.0815

Table B.4
Heat exchanger performance variables of the optimized WET engine during typical cruise conditions.

Parameter	Unit	Vaporizer	Condenser
$\dot{Q}$	MW	16.180	22.475
ΔT_{pinch}	K	73.8	10.6
Δp_{hot}	%	2.703	14.917
Δp_{cold}	%	0.003	2.851
ϵ	%	66.96	91.47

B.3. Take-off performance of the WET engine

Table B.5
Flow variables of the optimized WET engine during hot take-off conditions.

Station	p_0 (bar)	T_0 (K)	$\dot{m}$ (kg s^{-1})	FAR	WAR
AMB	0.843	293.2	1745.15	0.0000	0.000
2	0.867	295.6	1745.15	0.0000	0.000
24	1.128	320.7	70.79	0.0000	0.000
26	10.450	632.7	70.79	0.0000	0.000
28	42.477	944.4	70.79	0.0000	0.000
291	42.477	944.4	30.68	0.0000	0.000
292	42.477	944.4	6.44	0.0000	0.000
293	42.477	944.4	1.84	0.0000	0.000
294	42.477	944.4	−0.00	0.0000	0.000
3	42.477	944.4	40.12	0.0000	0.000
4	40.787	1952.4	58.53	0.0682	0.391
44	20.134	1556.9	82.77	0.0425	0.244
48	10.686	1363.3	87.37	0.0397	0.227
5	1.497	911.3	89.21	0.0386	0.221
6	1.469	551.9	89.21	0.0386	0.221
7	1.344	347.0	84.58	0.0386	0.156
9	1.324	347.0	84.58	0.0386	0.156
17	1.186	348.6	1674.35	0.0000	0.000
19	1.174	348.6	1674.35	0.0000	0.000
W1	1.344	347.0	4.63	–	–
W2	42.479	347.0	15.68	–	–
W3	42.477	587.8	15.68	–	–

Table B.6
Turbomachinery variables of the optimized WET engine during hot take-off conditions.

Parameter	Unit	Fan	IPC	HPC	HPT	IPT	LPT
$\dot{W}$	MW	57.261	22.719	24.199	24.199	22.719	57.261
π	–	1.4064	9.2656	4.0648	2.0257	1.8842	7.1383
η_{p}	–	0.9306	0.9121	0.9194	0.8983	0.9135	0.9231
τ	N m	306,386	27,934	20,952	20,952	27,934	306,386
Ω	rev/s	29.74	129.44	183.82	183.82	129.44	29.74
A	m^2	9.6261	0.3735	0.0588	0.0177	0.0451	0.0815

Table B.7
Heat exchanger performance variables of the optimized WET engine during hot take-off conditions.

Parameter	Unit	Vaporizer	Condenser
$\dot{Q}$	MW	42.052	34.257
ΔT_{pinch}	K	35.9	11.6
Δp_{hot}	%	1.888	8.491
Δp_{cold}	%	0.003	2.696
ϵ	%	63.68	91.61

References

[1] D.S. Lee, G. Pitari, V. Grewe, K. Gierens, J.E. Penner, A. Petzold, M.J. Prather, U. Schumann, A. Bais, T. Berntsen, D. Iachetti, L.L. Lim, R. Sausen, Transport impacts on atmosphere and climate: aviation, Atmosph. Environ. 44 (2010) 4678–4734. https://doi.org/10.1016/j.atmosenv.2009.06.005

[2] International Civil Aviation Organization, Annual Report of the Council to the Assembly, 2019. (accessed 12 February 2025), https://www.icao.int/annual-report-2019/.

[3] J. Kozuba, M. Ojciec, Overview of historical and future trends of commercial aircraft fuel efficiency, Acta Avionica 21 (2019) 12–17. https://doi.org/10.35116/aa.2019.0003

[4] International Civil Aviation Organization, ICAO Environmental Report 2016: On Board a Sustainable Future, 2016. (accessed 17 September 2025), https://www.icao.int/environmental-protection/Documents/ICAO%20Environmental%20Report%202016.pdf.

[5] V. Grewe, A. Gangoli Rao, T. Grönstedt, C. Xisto, F. Linke, J. Melkert, J. Middel, B. Ohlenforst, S. Blakey, S. Christie, et al., Evaluating the climate impact of aviation emission scenarios towards the Paris agreement including COVID-19 effects, Nat. Commun. 12 (1) (2021) 3841.

[6] O. Schmitz, H. Klingels, P. Kufner, Aero engine concepts beyond 2030: Part 1-the steam injecting and recovering aero engine, J. Eng. Gas Turbines Power 143 (2) (2021) 021001. https://doi.org/10.1115/1.4048985

[7] S. Kaiser, O. Schmitz, H. Klingels, Aero engine concepts beyond 2030: Part 2 - the free-piston composite cycle engine, in: Turbo Expo: Power for Land, Sea, and Air, 5 (2020), p. V005T06A018. https://doi.org/10.1115/GT2020-15395

[8] O. Schmitz, S. Kaiser, H. Klingels, P. Kufner, M. Obermüller, M. Henke, J. Zanger, F. Grimm, S. Schuldt, A. Marcellan, D. Cirigliano, P. Kutne, A. Heron-Himmel, S. Schneider, J. Richter, B. Weigand, A. Göhler-Stroh, A. Seitz, M. Hornung, Aero engine concepts beyond 2030: Part 3-experimental demonstration of technological feasibility, J. Eng. Gas Turbines Power 143 (2) (2021) 021003. https://doi.org/10.1115/1.4048994

[9] D.Y. Cheng, Parallel-compound dual-fluid heat engine (1976). US Patent 3,978,661.

[10] E.D. Larson, R.H. Williams, Steam-injected gas turbines, J. Eng. Gas Turbine Power 109 (1) (1987) 55–63. https://doi.org/10.1115/1.3240006

[11] K. Nishida, T. Takagi, S. Kinoshita, Regenerative steam-injection gas-turbine systems, Appl. Energy 81 (3) (2005) 231–246. https://doi.org/10.1016/j.apenergy.2004.08.002

[12] R. Pouzolz, O. Schmitz, H. Klingels, Evaluation of the climate impact reduction potential of the water-enhanced turbofan (WET) concept, Aerosp. 8 (3) (2021) 59. https://doi.org/10.3390/aerospace8030059

[13] S. Kaiser, O. Schmitz, P. Ziegler, H. Klingels, The water-enhanced turbofan as enabler for climate-neutral aviation, Appl. Sci. 12 (23) (2022) 12431. https://doi.org/10.3390/app122312431

[14] P. Ziegler, S. Kaiser, V. Gümmer, Parametric cycle studies of the water-enhanced turbofan concept, in: Turbo Expo: Power for Land, Sea, and Air, 5 (2023), p. V005T06A001. https://doi.org/10.1115/GT2023-100529

[15] P. Miltén, I. Johnsson, A. Lundbladh, C. Xisto, Generalized method for the conceptual design of compact heat exchangers, J. Eng. Gas Turbines Power 146 (111018) (2024) 1–11. https://doi.org/10.1115/1.4065922

[16] R.A. McDonald, J.R. Gloudemans, Open vehicle sketch pad: an open source parametric geometry and analysis tool for conceptual aircraft design, in: AIAA Scitech 2022 Forum, American Institute of Aeronautics and Astronautics, San Diego, CA, USA, 2022. https://doi.org/10.2514/6.2022-0004

[17] International Civil Aviation Organization, ICAO Aircraft Engine Emissions Databank (Version June 2025), 2025, (European Union Aviation Safety Agency). (accessed 8 September 2025), https://www.easa.europa.eu/en/domains/environment/icao-aircraft-engine-emissions-databank.

[18] M. Daly, Jane's Aero-Engines, Jane's Information Group, Coulsdon, UK, 30 edition, Coulsdon, UK, 2011.

[19] J. Kurzke, Fundamental differences between conventional and geared turbofans, in: Proceedings of the ASME Turbo Expo: Power for Land, Sea, and Air (GT2009), 1, 2009, pp. 145–153. https://doi.org/10.1115/GT2009-59745

[20] D.P. Raymer, Aircraft Design: A Conceptual Approach, American Institute of Aeronautics and Astronautics, Reston, VA, 6 edition, Reston, VA, 2018.

[21] R.A. McDonald, J.R. Gloudemans, Open vehicle sketch pad: an open source parametric geometry and analysis tool for conceptual aircraft design, in: AIAA SCITECH 2022 Forum, 2022, p. 0004. https://doi.org/10.2514/6.2022-0004

[22] International Aero Engines (IAE), LLC, Type-certificate Data Sheet No. IM.E.093, 2025, (European Union Aviation Safety Agency). (accessed 29 September 2025), https://www.easa.europa.eu/en/document-library/type-certificates/engine-cs-e/easaime093-pw1100g-jm-series-engines.

[23] D.L. Daggett, S. Ortanderl, D. Eames, J.J. Berton, C.A. Snyder, Revisiting water injection for commercial aircraft, in: World Aviation and Exposition. Reno, USA, 2004.

[24] D.L. Daggett, R.C. Hendricks, Water misting and injection of commercial aircraft engines to reduce airport NOx, Technical Report, 2004.

[25] A.G. Chen, D.J. Maloney, W.H. Day, Humid air NOx reduction effect on liquid fuel combustion, J. Eng. Gas Turbine Power 126 (1) (2004) 69–74. https://doi.org/10.1115/1.1615255

[26] O. Krüger, S. Terhaar, C.O. Paschereit, C. Duwig, Large eddy simulations of hydrogen oxidation at ultra-wet conditions in a model gas turbine combustor applying detailed chemistry, J. Eng. Gas Turbine Power 135 (2) (2013) 021501. https://doi.org/10.1115/1.4007718

[27] S. Göke, C. Paschereit, Influence of steam dilution on NOx formation in premixed natural gas and hydrogen flames, in: 50Th AIAA Aerospace Sciences Meeting Including the New Horizons Forum and Aerospace Exposition, 2012. https://doi.org/10.2514/6.2012-1272

[28] T. Grönstedt, Development of Methods for Analysis and Optimization of Complex Jet Engine Systems, Ph.D. thesis, Chalmers University of Technology, 2000.

[29] S. Gordon, B.J. McBride, Computer Program for Calculation of Complex Chemical Equilibrium Compositions and Applications. Part 1: Analysis, Technical Report, National Aeronautics and Space Administration, Cleveland, OH, 1994.

[30] J.R. Cooper, R.B. Dooley, Revised Release on the IAPWS Industrial Formulation 1997 for the Thermodynamic Properties of Water and Steam, The International Association for the Properties of Water and Steam, Lucerne, Switzerland, 2007.

[31] J.R. Cooper, R.B. Dooley, Release on the IAPWS Formulation 2008 for the Viscosity of Ordinary Water Substance, The International Association for the Properties of Water and Steam, Berlin, Germany, 2008.

[32] K. Duacik, R.B. Dooley, Release on the IAPWS Formulation 2011 for the Thermal Conductivity of Ordinary Water Substance, The International Association for the Properties of Water and Steam, Plzeň, Czech Republic, 2011.

[33] R.B. Dooley, Revised Advisory Note No. 3 - Thermodynamic Derivatives from IAPWS Formulations, The International Association for the Properties of Water and Steam, Prague, Czech Republic, 2018.

[34] M.T. Tong, I. Halliwell, L.J. Ghosn, A computer code for gas turbine engine weight and disk life estimation, in: Turbo Expo: Power for Land, Sea, and Air, 36061, 2002, pp. 111–118.

[35] J.-J. Korsia, G. De Spiegeleer, VITAL–European R&D programme for greener aeroengines, 18th ISABE (2007).

[36] G. Wilfert, J. Sieber, A. Rolt, N. Baker, A. Touyeras, S. Colantuoni, New environmental friendly aero engine core concepts, ISABE Paper 1120 (2007) 6.

[37] R. von der Bank, S. Donnerhack, A. Rae, M. Cazalens, A. Lundbladh, M. Dietz, Lemcotec: improving the core-engine thermal efficiency, in: Turbo Expo: Power for Land, Sea, and Air, 45578, American Society of Mechanical Engineers, 2014, p. V01AT01A001.

[38] R.C. Wilcock, J.B. Young, J.H. Horlock, The effect of turbine blade cooling on the cycle efficiency of gas turbine power cycles, J. Eng. Gas Turbines Power 127 (1) (2005) 109–120. https://doi.org/10.1115/1.1805549

[39] P. Miltén, I. Johnsson, A. Lundbladh, C. Xisto, GenHEX: a new heat exchanger design framework, in: Swedish Aerospace Conference, FT2025, 215, 2025. https://www.ecp.ep.liu.se/index.php/ft/article/view/1193.

[40] A. Johansson, P. Miltén, A. Lundbladh, C. Xisto, Modelling a hydrogen fuelled composite cycle aeroengine, in: Proc of the 34th Congr. of the Int. Counc. of the Aeronaut. Sci., 2024. https://www.icas.org/icas_archive/icas2024/data/papers/icas2024_1103_paper.pdf.

[41] C. Svensson, P. Miltén, T. Grönstedt, Modelling hydrogen fuel cell aircraft in suave, in: ICAS Proc., 2024. https://www.icas.org/icas_archive/icas2024/data/papers/icas2024_1078_paper.pdf.

[42] E. Hasselwander, I. Jonsson, A. Lundbladh, P. Miltén, C. Xisto, On the coupled integration of ducted heat-exchanger systems for aviation, in: Swedish Aerospace Conference, FT2025, 215, 2025. https://ecp.ep.liu.se/index.php/ft/article/view/1183.

[43] P. Miltén, I. Johnsson, A. Lundbladh, C. Xisto, Conceptual design exploration of hydrogen enhanced intercooling for future aeroengines, J. Eng. Gas Turbines Power 147 (121007) (2025) 1–12. https://doi.org/10.1115/1.4069483

[44] W.M. Kays, A.L. London, Compact Heat Exchangers, McGraw-Hill, Inc., New York, NY, 2 edition, New York, NY, 1955.

[45] VDI-Gesellschaft Verfahrenstechnik und Chemieingenieurwesen, VDI Heat Atlas, Springer-Verlag Berlin Heidelberg, New York, NY, 2 edition, New York, NY, 2010. https://doi.org/10.1007/978-3-540-77877-6

[46] P. Ziegler, C. Simson, T. Arzberger, A. Woitalka, F. Nöske, S. Kaiser, V. Gümmer, Water-enhanced turbofan condenser sizing considering configuration and operating conditions, Aeronaut. J. 129 (1336) (2025) 1494-1514. https://doi.org/10.1017/aer.2024.158

[47] S.M. Jeter, Effectiveness and LMTD correction factor of the cross flow exchanger: a simplified and unified treatment, in: ASEE Southeast Section Conference, 1 (2006), pp. 1–10.

[48] R. Storn, K. Price, Differential evolution–a simple and efficient heuristic for global optimization over continuous spaces, J. Glob. Optim. 11 (4) (1997) 341–359. https://doi.org/10.1023/A:1008202821328

[49] A. Ashraf, S. Pervaiz, W. Haider Bangyal, K. Nisar, A.A.A. Ibrahim, J.J.P.C. Rodrigues, D.B. Rawat, Studying the impact of initialization for population-based algorithms with low-discrepancy sequences, Appl. Sci. 11 (17) (2021) 8190. https://doi.org/10.3390/app11178190

[50] R.H. Byrd, P. Lu, J. Nocedal, C. Zhu, A limited memory algorithm for bound constrained optimization, SIAM J. Sci. Comput. 16 (5) (1995) 1190–1208. https://doi.org/10.1137/0916069

[51] T.H. Chilton, A.P. Colburn, Mass transfer (absorption) coefficients, Ind. Eng. Chem. 26 (11) (1934) 1183–1187.